Deployment Control of Spinning Space Webs and Membranes

by

Mattias Gärdsback

November 2008 Technical Reports from Royal Institute of Technology Department of Mechanics SE-100 44 Stockholm, Sweden

Akademisk avhandling som med tillstånd av Kungliga Tekniska Högskolan i Stockholm framlägges till offentlig granskning för avläggande av teknologie doktorsexamen måndagen den 8:e december 2008 kl 10.00 i F3, Kungliga Tekniska Högskolan, Lindstedtsvägen 26, Stockholm.
©Mattias Gärdsback 2008
Universitetsservice US-AB, Stockholm 2008

 $In\ the\ spider-web\ of\ facts,\ many\ a\ truth\ is\ strangled.$

Paul Eldridge (1888–1982)

Deployment Control of Spinning Space Webs and Membranes

Mattias Gärdsback Department of Mechanics, Royal Institute of Technology SE-100 44 Stockholm, Sweden

Abstract

Future solar sail and solar power satellite missions require deployment of large and lightweight flexible structures in space. One option is to spin the assembly and use the centrifugal force for deployment, stiffening and stabilization. Some of the main advantages with spin deployment are that the significant forces are in the plane of rotation, a relatively simple control can be used and the tension in the membrane or web can be adjusted by the spin rate to meet the mission requirements. However, a successful deployment requires careful development of new control schemes.

The deployment rate can be controlled by a torque, applied either to a satellite in the center or by thrusters in the corners, or by deployment rate control, obtained by tether, spool braking or folding properties. Analytical models with only three degrees of freedom were here used to model the deployment of webs and membranes for various folding patterns and control schemes, with focus on space webs folded in star-like arms coiled around a center hub. The model was used to investigate control requirements and folding patterns and to obtain optimal control laws for centrifugal deployment. New control laws were derived from the optimal control results and previously presented control strategies. Analytical and finite element simulations indicate that the here developed control laws yield less oscillations, and most likely more robustness, than exixting controls.

Rotation-free (RF) shell elements can be used to model inflation or centrifugal deployment of flexible memebrane structures by the finite element method. RF elements approximate the rotational degrees of freedom from the out-of-plane displacements of a patch of elements, and thus avoid common singularity problems for very thin shells. The performance of RF shell elements on unstructured grids is investigated in the last article of this thesis, and it is shown that a combination of existing RF elements performs well even for unstructured grids.

Keywords: Centrifugal force deployment; Spin deployment; Space web; Flexible Structures; Rotation-free; Shell element.

Contents

Nomeno	elature	ix
Chapte	1. Introduction	1
1.1.	Overview	1
1.2.	Scope and aims of thesis	2
1.3.	Outline of thesis	2
Chapte	2. Background	4
2.1.	Some applications of large space structures	4
2.2.	Deployment and stabilization techniques	8
Chapte	3. Modelling	16
3.1.	Fundamental laws	16
3.2.	Analytical model	17
3.3.	Optimal control	23
3.4.	Finite element model	27
3.5.	Elements for membrane modelling	35
Chapte	4. Results	39

viii CONTENTS

4.1.	Summary of the most important results from papers $1-3$		
4.2.	Summary of the most important results from paper 4	45	
Chapter	5. Conclusions	49	
5.1.	Centrifugal force deployment	49	
5.2.	Rotation-free elements	50	
Chapter	6. Future research	51	
6.1.	Centrifugal force deployment	51	
6.2.	Rotation-free elements	51	
Acknowl	edgment	52	
Bibliogra	aphy	53	
List of pa	apers	63	
Paper 1:	Design Considerations and Deployment Simulations of Spinning Space Webs		
D 0.	Dealess of Control of Colonia of Control of Colonia of Control of		

Paper 2: Deployment Control of Spinning Space Webs

Paper 3: Optimal Deployment Control of Spinning Space Webs and Membranes

Paper 4: A Comparison of Rotation-Free Triangular Shell Elements for Unstructured Meshes

Nomenclature

```
A
         cross-sectional area
E
         Young's modulus
\boldsymbol{F}
         force vector
         moment of inertia for the center hub
J
L
         current arm length
         length to mass dm
l
M
         torque
m
         mass
N
         tensile force in arm
         number of arms or nodes
n
         number of peripherical nodes
p
\boldsymbol{R}
         position vector
         radius vector
r
S
         side length of web
         sign of i
S_i
         vector of control variables
\boldsymbol{u}
         velocity
v
         vector of state variables
\boldsymbol{x}
         vector of state and control variables
\boldsymbol{y}
\mathcal{E}
         energy
         {\it kinetic\ energy}
\mathcal{K}
\mathcal{L}
         angular momentum
\mathcal{P}
         power
Greek\ Symbols
         \phi + \varphi
\alpha
         engineering strain
ε
         mass per length
\gamma
         rotation angle of hub
         density function
\rho
         arm coiling angle
         angle between arm and radial direction
         angular velocity (of hub)
Subscripts \\
         initial time
```

x Nomenclature

```
 \begin{array}{lll} c & \text{corner} \\ ca & \text{cable} \\ f & \text{final time} \\ h & \text{hub} \\ w & \text{web} \\ Superscripts \\ (i) & \text{coordinate system } i \end{array}
```

CHAPTER 1

Introduction

1.1. Overview

The trend in the space industry is to build successively larger structures. The interest in extremely large structures is also likely to increase in the future with the development of promising applications like solar power satellites (SPS) or solar sails. Solar sails use the solar radiation pressure as propulsion, which makes intergalactic exploration possible with little mass required for fuel. The idea of an SPS is to collect solar energy in space and beam it to Earth, which could possibly contribute to solve the electricity demand on our planet. To enable this, the mechanically deployed and rigidized structures used today must be replaced with lighter and more flexible solutions. Two interesting concepts used for deployment and stiffening of large flexible structures in space is to use pressurized air to inflate structures or to take advantage of the centrifugal forces in a rotating structure.

Many inflatable structures have been deployed successfully in orbit, e.g. the Echo balloons [31] in the 1960's and the Inflatable Antenna Experiment (IAE) [41] in 1996. Even though spin-stabilized satellites have been developed since the birth of space exploration, the only successful centrifugal deployment of a large structure in orbit was the Russian Znamya-2 reflector [103] in 1993. The follow up-experiment Znamya 2.5 failed due to entanglement. In 2004, Japanese ISAS successfully deployed two prototype sails, a 10 m clover type sail and a fan type sail, using centrifugal forces and zero gravity provided by a sounding rocket [110, 154]. In 2005, Cosmos 1 was planned to be the first controlled flight of a solar sail, but the launch rocket exploded prior to the deployment. In August 2008, another launch failure stopped NASA's NanoSail-D mission [1]. Instead, the Solar Polar Imager experiment [3], scheduled to 2012, is probably going to be the first mission that will use solar sail technology. The launch cost, and thus the initial investment, of SPS is still too high to make it feasible, even though it is under continuous investigation by NASA, JAXA and ESA. The conditions are different in space than on Earth and small scale experiments do only give half the truth for structures of this size. The development of simulation methods is therefore crucial before the launch of full-scale experiments.

The ESA Advanced Concepts Team has investigated several methods to deploy and stabilise large lightweight structures for solar power satellite systems: swarm-intelligence based automatic assemblys, formation flying of a large number of elements and "Furoshiki"-type approaches. The original Furoshiki concept is taking advantage of formation flying properties, but adds stability since the satellites are loosely connected by a web or a membrane. However, a first attempt to deploy

1

a web in a sounding rocket experiment failed [118]. A simpler and more robust deployment concept is therefore required.

1.2. Scope and aims of thesis

This project was started in collaboration with the ESA Advanced Concepts Team and the aim was to investigate deployment of space webs from spinning satellites. The main scope of this thesis is the dynamics and control of such deployments, mainly for space webs but also for membranes. A major goal is that the final control law should be as simple and robust as possible. A deployment is strongly dependent on the initial folding of the structure being deployed, but the actual folding is only briefly covered in this thesis. Instead, web architectures and folding patterns for centrifugal deployment were analyzed and presented in an ESA report [150], which was also part of my licentiate thesis [45]. In the present thesis, the folding pattern that was then identified as the most suitable for space webs, i.e. the web folded into star arms coiled around the center hub, gain most interest. An analytical and a finite element (FE) model are developed, and simulation results from the models are presented. The analytical model does not differentiate between webs and membranes, so the results are valid also for membranes. With small modifications, the model is also valid for many other common folding patterns. The analytical model can be used to obtain optimal control strategies. Optimal control is performed to achieve control laws for spin deployment of space web and membranes. The stabilization of already deployed webs is not in the scope of this thesis.

FE modelling of very thin membrane structures in general, and inflatable structures in particular, requires efficient and rapidly computed elements. A minor part of this thesis is about a class of such elements, rotation-free (RF) shell elements. RF elements do only use translational degrees of freedom (DOFs), and therefore, bending can be taken into account without introducing any extra DOFs compared to a membrane element. The efficiency of RF elements has only been proven for regular grids. The aim of the last part of this thesis was to investigate if RF formulations are accurate also for unstructured grids and if possible improve the existing RF elements.

1.3. Outline of thesis

The first part of this thesis includes a short background on applications for centrifugally deployed webs and membranes and technologies to deploy and stiffen lightweight structures in space. Not all applications and not all methods are presented, only the ones that are of interest for the rest of the thesis. Then follows

a description of the different methods and models we have used to model the dynamical behaviour and to optimize the behaviour in terms of controllability. The most important results and conclusions from the four articles that are presented in the end of the thesis are briefly described. At the end, the articles are included, as published or submitted, but typeset in the same format.

CHAPTER 2

Background

2.1. Some applications of large space structures

2.1.1. Solar power satellites. The idea behind SPS¹ is to collect solar energy in space and beam it to antennas on Earth. The main advantages are the unobstructed view of the Sun, unaffected by the day/night cycle, weather or seasons and that the rectifying antenna (rectenna) on Earth can be smaller than solar cells with the same capacity. The main disadvantages are the high launch cost to put the required materials in space and the lack of experience on projects of this scale in space.

An SPS essentially consists of three parts: (i) a means of collecting solar power in space, e.g. via photovoltaic (PV) solar cells or a heat engine, (ii) a means of transmitting power to Earth, e.g. via microwave or laser, and (iii) a means of receiving power on Earth, e.g. via a microwave antenna. The large spatial structures must be lightweight and built in geostationary orbit from a tightly packed launch configuration.

The SPS concept was introduced in 1968 by Peter Glaser [54], who was also granted a US patent [55] in 1973 for his method and apparatus to collect solar radiation energy in a geostationary orbit and convert it to microwave energy, that is beamed to Earth by microwave power transmission to get electrical power for distribution. During 1978–1981, NASA and the US Department of Energy jointly organized an extensive feasibility study that investigated, e.g. resource (materials, energy and rectenna sites) requirements, space transportation, power transmission and reception, financial scenarios, meteorological effects, public acceptance and regulations. The studies were concentrated on the enormous SPS Reference System [112] with a 5 GW power output, a collector array of 5 km x 10.5 km and a rectenna of 10 km x 15 km. A net energy analysis calculated that this type of SPS could be a net energy producer [67]. The summary assessment [143] of the project concluded that the SPS had the potential to become an important source of electric power, but the initial investment cost was far too high and there were still too many uncertainties in technology and environmental effects.

During 1995–1996, NASA [90] conducted a re-examination of technologies, system concepts and markets for a future SPS. One of the key concepts that were developed was the Suntower SPS [91], which could be deployed in low or middle Earth orbit

¹SPS is an abbreviation for solar power satellite, space power satellite, satellite power system. It is also commonly referred to as SSP, i.e. space solar power, space-based solar power or satellite solar power. Peter Glaser originally referred to it as "power from the sun".

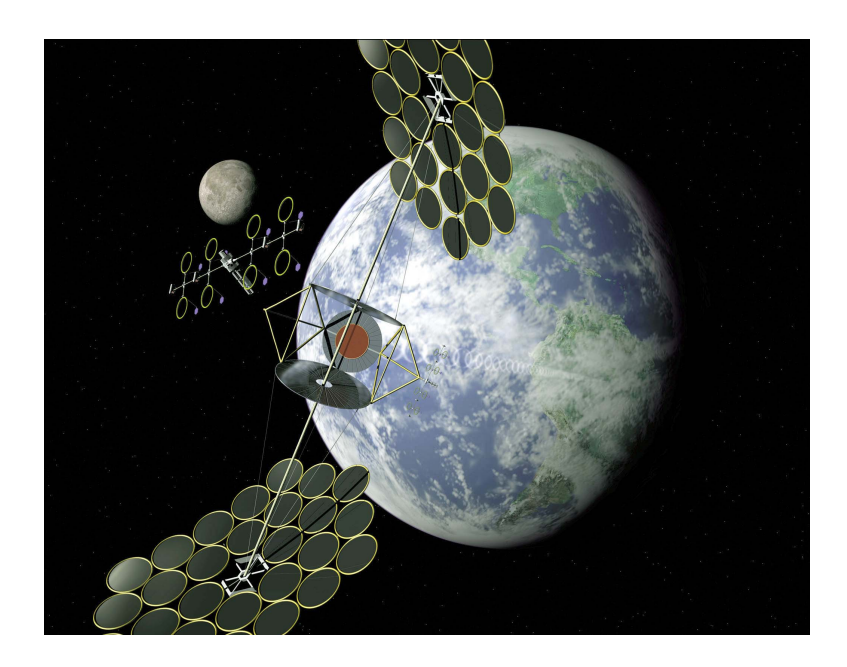


FIGURE 2.1. Solar Power Satellite (Courtesy of NASA).

and use a series of identical smaller arrays. This facilitates the space transportation and reusable launch vehicles can be used. Mankins [91] estimates that the initial investment could be reduced by a factor of 30:1 for these smaller SPS systems, and predict that even though a large GEO-based SPS have the potential for higher financial returns in the long run, small SPS systems will reach space first. The "Fresh Look" study was followed by a series of NASA sponsored satellite solar power (SSP) studies: an SSP concept definition study in 1998, the SSP Exploratory Research and Technology (SERT) program in 1999–2000 and the SSP Concept and Technology Maturation (SCTM) program 2001–2002. In all the three studies, the focus was on identifying system concepts, architectures and technologies that may lead to a practical and economically viable SPS system; a summary is found in [102]. A recent state-of-the-art article of SPS [89] reviews a number of SPS concepts and identifies key issues for SPS to become economically viable.

Matsumoto [95] reviews early Japanese research on solar power satellites, with emphasis on microwave power transmission (MPT), and concludes that the center of MPT technologies shifted to Japan in the 1980's and 1990's. Oda [120] concludes that the main challeges to overcome for the SPS are: (i) developing a low-cost and powerful space transportation system, (ii) designing a lightweight SPS, (iii) allocating frequency for the energy transmission and (iv) alleviating people's concerns about environmental and health effects. A recent summary of JAXAs SPS concept



FIGURE 2.2. Solar sail demonstration (Courtesy of NASA).

is found in [138], where a roadmap of a stepwise approach to achieve a commercial SPS around 2030 is presented. The first step was initiated in February 2008 when a satellite was launched to demonstrate the microwave power transmission system in small scale (order of $10~\rm kW$ compared to GW for full scale).

The European Space Agency, in the frame of its Advanced Concepts Team, started an SPS programme in 2002, and the viability of the SPS for Europe was presented in [148]

2.1.2. Solar sails. Solar sails or light sails are a proposed form of spacecraft propulsion that take advantage of the kinetic energy in the light from the Sun or other light sources. Large membrane mirrors reflect the photons and because of conservation of momentum a small thrust is provided. However, the acceleration is small and it takes months to build up useful speeds. The radiation pressure at Earth is about 10^{-5} Pa and decreases by the square of the distance from the Sun. It follows that a solar sail must be very large and the payload must be very small.

Kepler vaguely proposed the idea of sailing in space already in the 17th century. In 1873, Maxwell demonstrated that sunlight exerts a small pressure as photons bounce off a reflective surface. According to McInnes comprehensive book on solar sails McInnes:1999, the Russian scientists Tsiolkovsky and Tsander first introduced the idea of a practical solar sail, as they in the 1920's both wrote of using large lightweight mirrors to collect the pressure of sunlight for use as propellant in cosmos. In 1958, Garwin [50] authored the first solar sail paper in a western scientific paper. The same year, Cotter [26] was publicly known when his ideas on solar sails

were picked up by Time Magazine. NASA began technology studies in the mid-1960's. McNeal and Hedgepeth developed the the helicopter-like Heliogyro concept in 1967 [66,87]. With the aim of a rendez-vouz with Halley's comet, NASA conducted a first profound study in 1977–78 [42], which investigated square sails and the Heliogyro and concluded that solar sailing was a feasible spacecraft-propulsion technique.

In 1974 the principles of solar sailing were demonstrated for the first time in space when the Mercury and Venus-explorer Mariner 10 ran low on attitude control gas [145]. Instead it aligned its solar arrays towards the Sun to use the low solar radiation pressure for attitude control. This technique is still used, the geostationary communications satellites Eurostar E3000 and Intelsat use small solar sails and gyroscopic momentum wheels for on-station attitude control [156]. In 1984, Forward [39] proposed to use solar-powered laser power systems with 1000-km-diameter to push light sails of 3.6-km-diameter for missions to α -Centauri. Laser-propelled light sails have low energy efficiency and extremely large lenses are required, two problems that can be decreased by particle beams, instead of light beams, reflected by a magnetic field on the spacecraft [82]

To date, no solar sail has been successfully deployed in space as a primary means of propulsion. Cosmos 1, a joint private project between the Planetary Society, Cosmos Studios and the Russian Academy of Science, was planned to be the first solar sail in orbit in 2005, but the spacecraft it would have been launched from failed to reach orbit. In August 2008, another launch failure stopped NASAs NanoSail-D mission [1]. Cosmos 1 is planned to be followed by Cosmos 2 and the possibilities for a future launch of a flight spare of NanoSail-D are under investigation.

Several solar sail roadmap missions [64] are envisioned as part of the NASA In-Space Propulsion Technology Program . A near-term mission is the Heliostorm warning mission [164], where propellantless thrust is required to hover indefinitely at the L1/Heliostorm point. Another interesting mission is the Solar Polar Imager mission (SPI), where a 160 × 160 m² square sail is planned to be launched in 2013 [27]. The aim of the SPI is to study the solar poles and find new knowledge about the solar corona, solar cycle and the origins of solar activity. The development and ground demonstration of two 20 m quadratic solar sails, Fig. 2.2, developed by ATK space systems and L'Garde, that can possibly be scalable to the required sizes, are described in [74]. The ESA is also considering a similar solar sail mission, the Solar Polar Orbiter [98]. It has been proven theoretically that a spacecraft powered by solar sails can escape the solar system with a cruise speed higher than for a spacecraft powered by a nuclear electric rocket system. NASA has considered solar sails for a future interstellar probe [94].

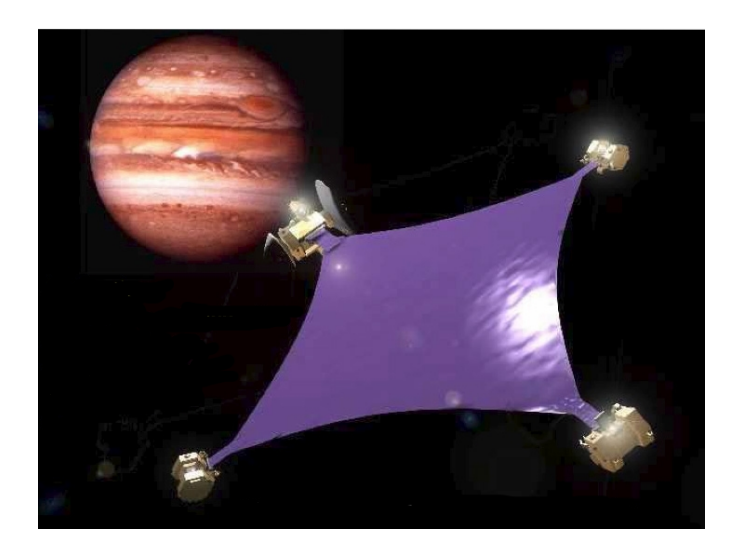


FIGURE 2.3. The Furoshiki Space Web (Courtesy of JAXA).

2.2. Deployment and stabilization techniques

2.2.1. The Furushiki project. A space web is composed of a large membrane or net held in tension by thruster-controlled corner satellites, Fig. 2.3, or by spinning the whole assembly. The web tension gives the required geometric out-of-plane stiffness so that the web can serve as a platform for large apertures, such as a phased antenna or an SPS. The space web concept was developed by Nakasuka et al. [115-117] for the "Furoshiki satellite". An idea put forward by Kaya et al. [78] is to build up a structure on the web by robots that crawl on the web like spiders, Figure 2.4. In January 2006, the Institute of Space and Astronautical Science (ISAS) in Japan, in collaboration with the University of Tokyo and the Vienna University of Technology, conducted the first "Furoshiki experiment" in simulated zero gravity by launch with a sounding rocket. The plan was to deploy a very thin 130 m² triangular space web to test the deployment feasibility and the function of the robots. The difficulty in deploying a space web in a controlled manner became evident in the partly chaotic deployment. Three corner satellites were released radially by separation springs from a central satellite. Thruster control was applied on the corner satellites to reduce the repulsion force at full deployment and for attitude control. However, the web entangled due to out-of-plane motions. communication problems between the central satellite and the corner satellites and a too rapid deployment [118].

Also the ESA Advanced Concepts Team has investigated the possibilities to construct large space antennas and SPSs in orbit. One method is to use a Furoshiki



FIGURE 2.4. Crawling robot Roby Space III (Junior) on web (Courtesy of ESA).

space web [71], but to use a simpler and more robust control. Web design and folding pattern for centrifugal force deployment of space webs, and mathematical models to simulate controlled and uncontrolled deployment were developed in [150] and summarized in [49] with focus on the simulations. The dynamics and control of the deployment was further investigated in [48]. The dynamics and control of a deployed web, with crawling spider robots, have been investigated by the University of Glasgow in a parallel study [100, 101]. The stability of deployed webs is also the subject of [127].

2.2.2. Use of centrifugal forces. The interest in large space structures deployed and stabilized by centrifugal forces increased in the 1960's when Astro Research Corporation analyzed several spin-stabilized structures [65, 66, 81, 83, 87, 133, 141, 142]. One concept is the Heliogyro solar sail, e.g. [66, 87, 88], which has been the subject of in-depth analysis since its introduction by MacNeal [87] in 1967. The Heliogyro uses the same principles as a helicopter for attitude control, but with no rigid boom structure for the rotor blades. Instead, these are made of thin film and stiffened by rotating the spacecraft. The 1 to 3 meters wide sheets are stowed in rolls, which simplifies the folding, packaging and deployment. Centrifugal force is selected as the preferred method for rigidising the long narrow sails on the basis of minimum weight and minimum complexity [99, 162].

The feasibility studies of a large-aperture paraboloidal-reflector low-frequency telescope (LOFT) [65, 141], Figure 2.6, provide important information on deployment

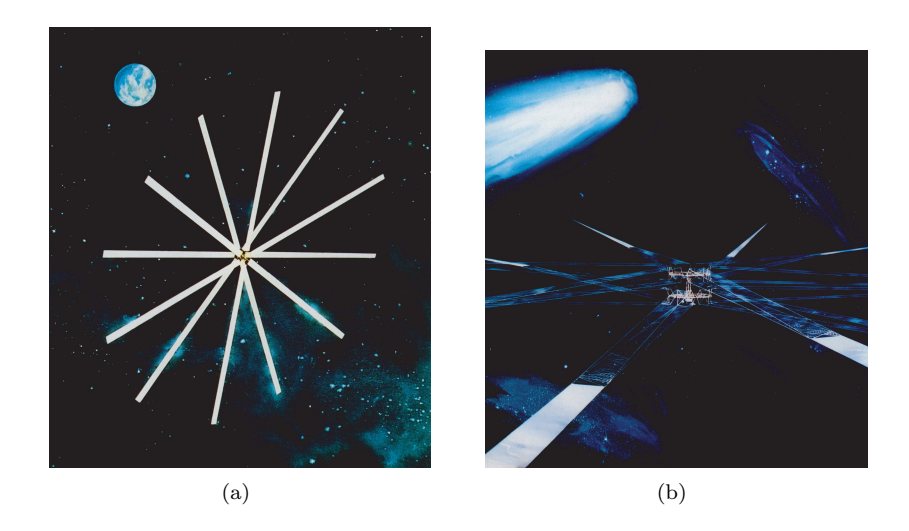


FIGURE 2.5. The Heliogyro solar sail, [147].

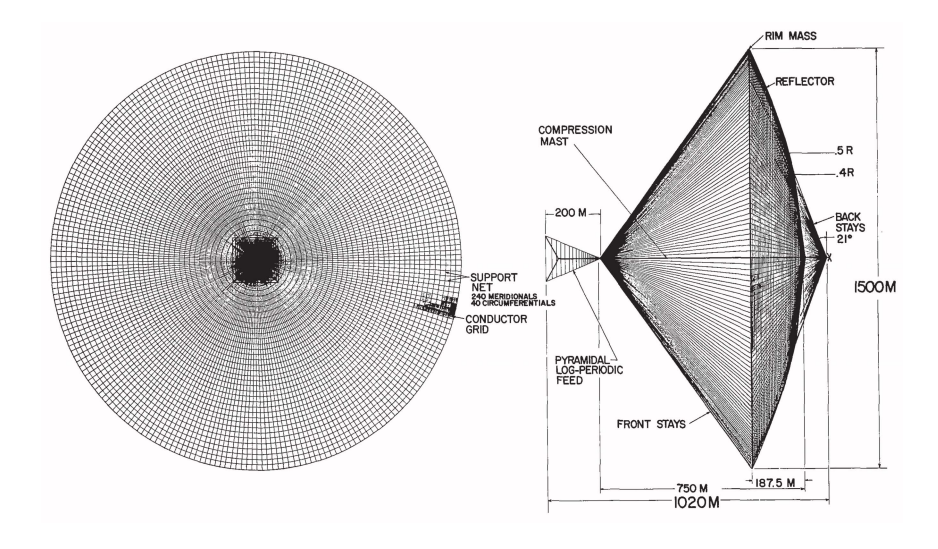


FIGURE 2.6. The baseline design of the LOFT concept, [141].

controllability aspects. The deployed size is of the reflector is 1500 m in diameter and 1020 m in height, while the stowed size is only 5.5 m and 5.9 m, respectively. During the first phase, which occupies 95% of the 3-hours deployment time, a constant torque provides the total angular momentum, but the deployment velocity is small so only 60% of the reflector is deployed. Then the torque is turned off rapidly and the tensile force in the spools is decreased so that the reflector is deployed

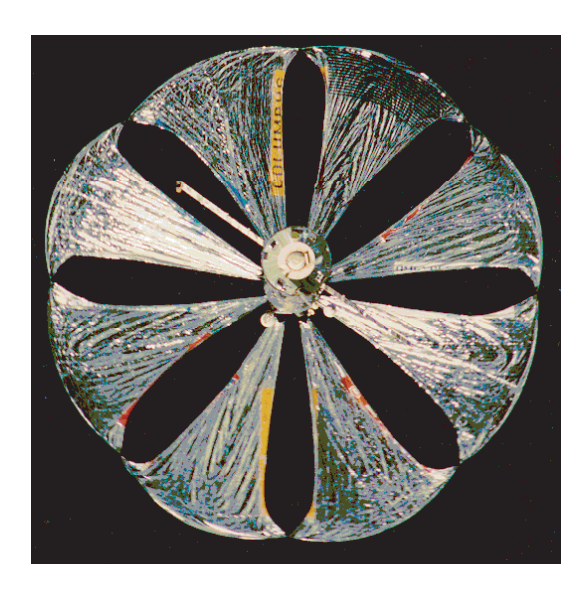


FIGURE 2.7. Znamya-2 deployment test (Courtesy of Russian Federal Space Agency).

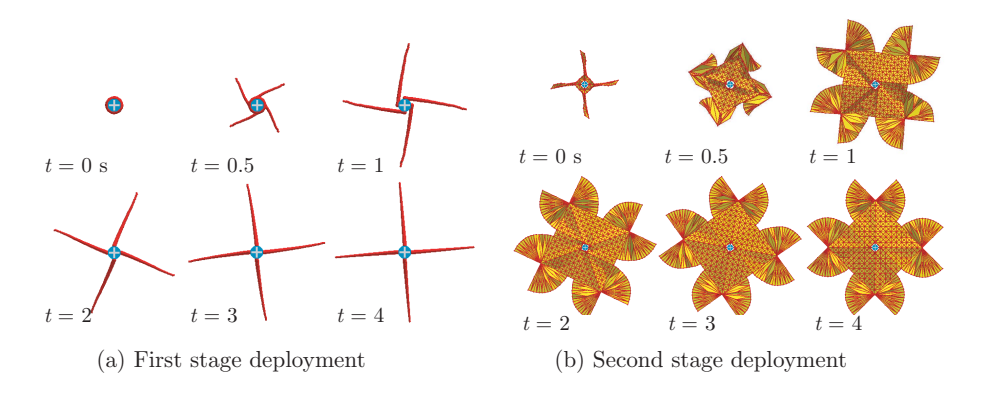


FIGURE 2.8. Deployment of the clover type solar sail, [110].

rapidly. The final angular velocity of 0.09 rpm was selected as a compromise: fast enough to generate sufficient tensile stresses in the net and to avoid dynamic coupling with the slower orbital frequency at an altitude of 6000 m, but slow enough to keep the demand for orientation control torques at tolerable levels [141].

The only successful deployment and control of a large spin-stabilized space structure is the Znamya-2 reflector, which was launched from a resupply vehicle from the Russian MIR space station in 1993 [103], Figure 2.7. The 20-m-diameter reflector was folded in a star-like pattern and deployed in two separate steps using torque

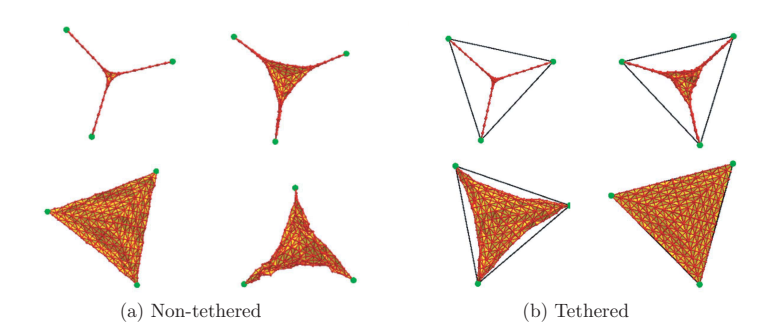


FIGURE 2.9. Deployment of triangular sail: (a) without tethers and (b) with tethers, [97].



FIGURE 2.10. Deployment of quadratic solar sail, [96].

and spool velocity for control. The torque was provided by an expandable counterrotating flywheel connected to an electric motor. In 1999, the deployment of a 25-m-diameter mirror in the follow-up experiment Znamya 2.5 failed because the membrane got caught in an antenna. A mission operations software was to blame [58]. To avoid similar future failures Shpakovsky [146] proposes to first deploy the flexible membrane package radially away from the spacecraft by inflatable tubes until the centrifugal force is sufficiently large, and then let the rotational inertia forces act alone. Kishimoto et al. [79] use a similar approach.

Many solar sail concepts use spin deployment and stabilization, e.g. the Interstellar Probe Mission [140, 158] and the UltraSail [17], where gas thrusters are planned to

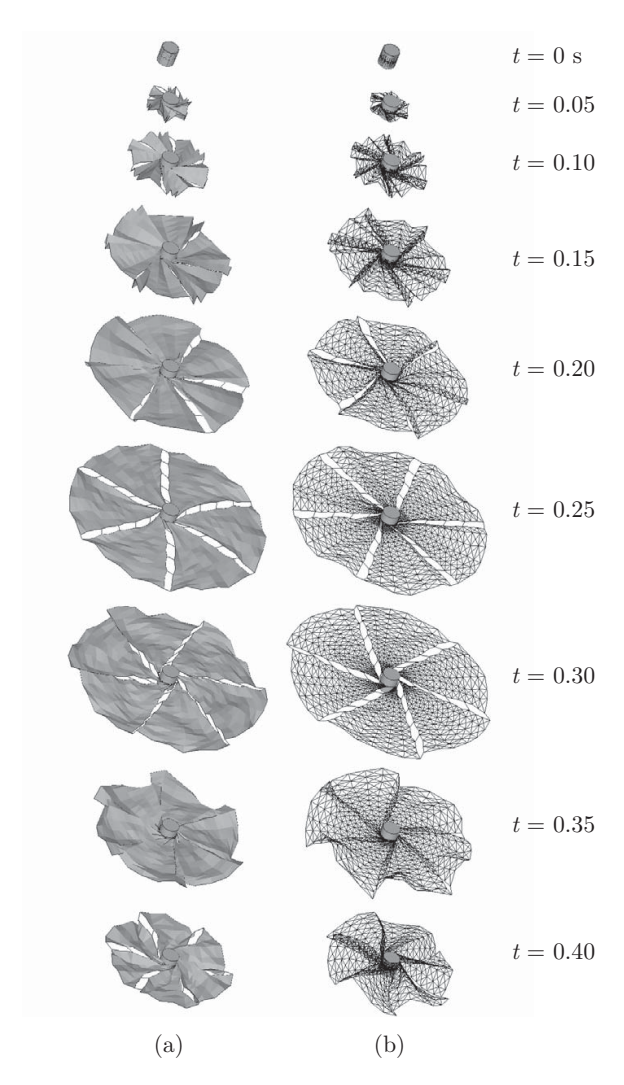


FIGURE 2.11. Deployment simulations by Miyazaki and Iwai using (a) membrane elements and (b) masses and springs, [106].

spin up spacecrafts to deploy and stabilize sails with 410 m and 1 km diameters, respectively.

Recently, Japanese researchers have also analyzed and tested, both on ground and in space, several spin solar sail concepts [5, 44, 69, 93, 96, 97, 104, 105, 107–109, 113, 114, 119, 121, 152–154]. In 2004, ISAS successfully deployed two prototype sails, a 10 m clover-type sail and a fan-type sail, using centrifugal forces in the simulated

zero gravity provided by a sounding rocket [110, 154]. The clover-type sail has a quadratic main sail with two fan parts and a mass in each corner. The sail is folded in a star-like pattern and deployed in two stages, Figure 2.8. Mori *et al.* [110] perform two deployment experiments: a spinning table in ambient environment and an in-orbit experiment using a sounding rocket. The diameter of the sail for the ground experiment is 2.5 m, whereas it for the sounding rocket experiment is 10 m. The ground experiments show that the coiling off-coiling on phenomenon did not occur due to the air resistance, so in-orbit experiments are required. To prevent re-coiling of the sail around the centre hub, a one way clutch mechanism is used. If the centre hub rotates faster than the tip of the sail, the clutch is locked, whereas if the tip rotates faster, the clutch is slipping so that the motions of the sail and centre hub are uncoupled. The stick-slip clutch is a simple passive way to achieve a controlled deployment for a small membrane.

Matunaga et al. [93,97] introduced a solar sail system composed of three corner satellites connected by tethers and a large triangular film surface, Figure 2.9. The sail is folded in three radial arms rolled up on the corner satellites. During deployment, the length between the corner satellites are controlled by the tethers, which take all the tension. Ground experiments with membranes with side length 1.76 m with air thrusters on the corner satellites and simulations using a mass–spring model were performed. The advantage of having tethers connecting the corners was shown, Fig. 2.9. Matunaga et al. [96] previously analysed the deployment of a 30×30 m² quadratic sail with radial tethers. Length control and a combination of length control in the beginning and tension control in the end yielded stable deployments, Fig. 2.10, while no control or tension control yielded the usual coiling off-coiling on phenomenon.

Onoda et al. [126] investigated analytically a constant angular velocity-deployment and stabilization of a spinning solar sail and verified the concept by a 2.2–mdiameter model experiment under gravity and normal air pressure. Miyazaki and Iwai [106] developed a mass–spring network model for the simulation of the deployment phase of a spinning solar sail. A comparison is made between membrane and mass–spring simulations of torqueless deployment for a 2-m-diameter solar sail, Fig. 2.11. Because no torque is applied, the web is first coiled off from the center hub and then coiled back onto the hub. Kanemitsu et al. [76] also investigated self-deployment, in their case of a 2-metre-diameter antenna by experiments in water, to simulate zero gravity, and by multi-body modelling.

2.2.3. Inflatable structures. Another method to deploy and rigidize large lightweight structures in space is to use pressurized air for inflation of membranes. Inflatable structures have several important advantages compared to more traditional structures, e.g. low mass, storage volume and cost, mechanical simplicity,

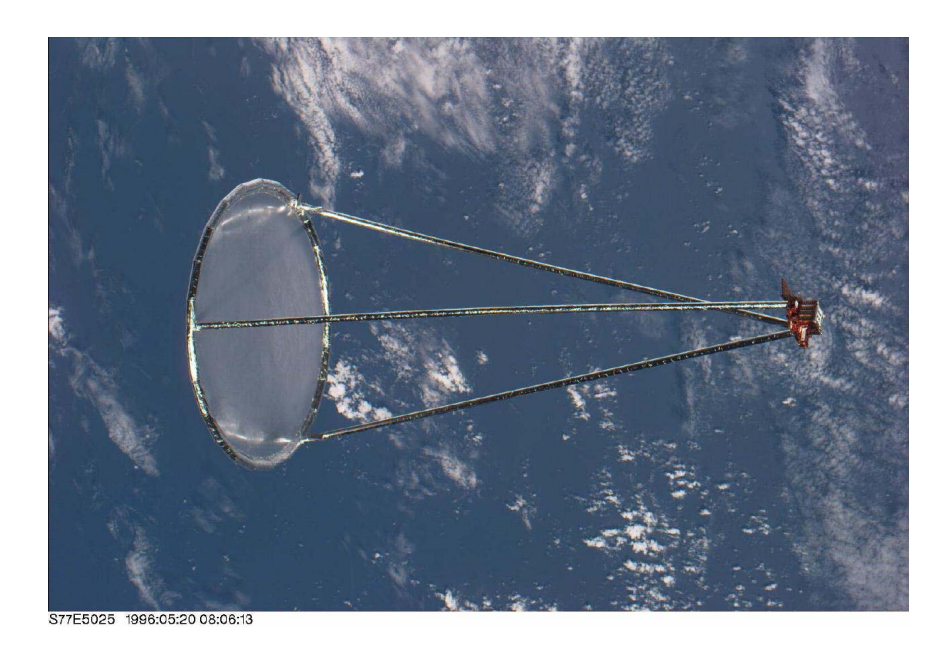


FIGURE 2.12. The Inflatable Antenna Experiment (Courtesy of L'Garde).

good thermal properties and damping [139]. Still, the use of large inflatable structures in space has been scarce so far, since deployment reliability is not yet proven because ground testing in relevant conditions is difficult to achieve, and reliability is one of the most important issues for space applications. Good dimensional accuracies have been obtained in ground test systems, and what remains is to prove their long-term strength and survivability in the space environment [18].

There has been an interest in inflatable structures since the 1950's. Relatively small inflatable space decoys have become operational because of their low weight and ease of packaging. Early developments of large structures, such as the Echo balloon series focused on demonstrating the potential of inflatable structures in orbit. The Echo balloons were large metallic balloons designed to act as passive reflectors for communication signals. L'Garde has pioneered the development of inflatable technology and an overview of their research until 1995 is found in [18]. Its most advanced structure being deployed so far is the IAE launched in 1996 [40], a 14-m-diameter antenna supported by three 28 m long struts, Fig. 2.12. Although the expected final state was obtained, the deployment did not follow the anticipated sequence. More about past experiments and developments of inflatables can be found in, e.g. the two first chapters of Ref. [72]. Jenkins has compiled two comprehensive books in the exciting field of Gossamer structures [72, 73]. A recent review article by Inman [70] also describes the state of the art.

Modelling

3.1. Fundamental laws

The deployment of a rotating web or membrane can be restricted to rotation in a plane and rotation about the symmetry axis. The angular momentum, \mathcal{L} , the angular velocity, ω , and the torque, M, are all directed along the symmetry axis, and can be regarded as scalars and only the moment of inertia, J, about the symmetry axis is required. For this system, \mathcal{L} is

$$\mathcal{L} = J\omega \tag{3.1}$$

and the kinetic energy, K, is

$$\mathcal{K} = \frac{J\omega^2}{2} \tag{3.2}$$

The dynamics of a closed rotating system is governed by the fundamental laws of conservation of angular momentum and conservation of energy. If no external torque is applied, Eq. (3.1) yields the final angular velocity as

$$\omega_f = \frac{J_0}{J_f} \omega_0 \tag{3.3}$$

where 0 denotes the initial time and f the time when the deployment is finalized. Notice also that the energy, \mathcal{E} , is conserved, but generally not the kinetic energy \mathcal{K} . However, for our model no energy dissipates. For an expanding system $J_f \gg J_0$, and consequently $\omega_f \ll \omega_0$. Expressions for J_0 and J_f for a system with a hub, corner masses, and web or membrane are given in [48,150]. An external torque, M, about the symmetry axis changes the angular momentum according to

$$\dot{\mathcal{L}} = M \tag{3.4}$$

and the power of the torque is

$$\mathcal{P} = \dot{\mathcal{E}} = M\omega \tag{3.5}$$

There are many interesting implications of these equations. If no external torque is used, most of the initial energy must be removed somehow and ω_f would be small, which makes a torque-free deployment infeasible [48]. A counter-rotating flywheel could be used to provide the torque [103]. A flywheel with high ω_0 cannot be used because the initial energy must be removed in some way [103]. The power required to spin up the smaller flywheel is much higher than for the hub [48], but much of the excessive kinetic energy can be stored in the flywheel.

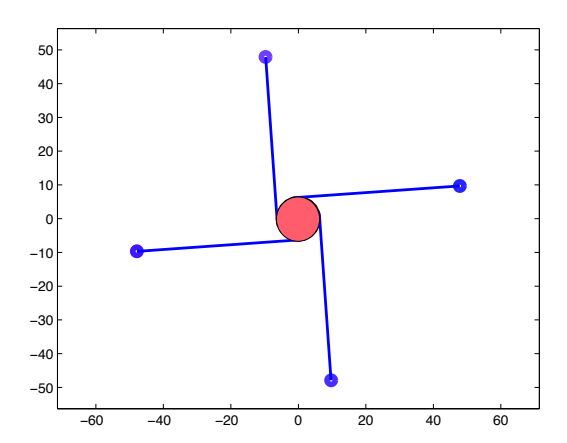


FIGURE 3.1. Visualisation of the analytical model.

3.2. Analytical model

Simple analytical models can be used to describe the deployment dynamics qualitatively. The development of our analytical model follows the same principles that Melnikov and Koshelev [103] use to describe the deployment of split and solid reflectors and tether systems from a rotating central satellite. Hedgepeth [65] also use a similar model for the LOFT system. The following assumptions were made:

- Out-of-plane torques and motions were not included. Thus, the problem was two-dimensional.
- The arms were supposed to be straight and deployed symmetrically relative to a symmetrical axis.
- Effects of the hub orbit or hub direction in the orbit were not considered.
- The gravity gradient and the elasticity in the cables were neglected.
- Energy dissipation caused by deformation, friction and environmental effects were neglected.

The above assumptions lead to an axisymmetric problem, Fig. 3.1. Similar models have also been used for optimal control of tether deployment and retrieval of a subsatellite from a shuttle in Keplerian orbit [6, 43, 160, 161]. For the tether models, the spacecraft is in orbit and the gravity gradient is included, but it is still an easier model to solve because the spacecraft has a constant angular velocity relative to origin (Earth).

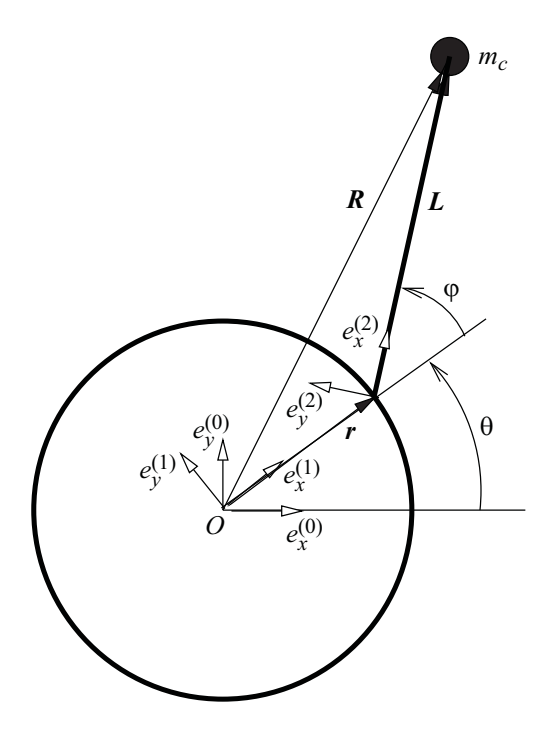


FIGURE 3.2. The analytical model for a point mass.

3.2.1. Equations for straight arms. Three equations are required to solve for the three unknown DOFs. Here, the change of angular momentum for the hub and two equations of motion for the arms in the plane of rotation are available. The change in angular momentum, due to the applied external torque and the torque exerted by the pulling arms, for the central hub in Fig. 3.2 or 3.3 is

$$\dot{\mathcal{L}} = M + n(\mathbf{r} \times \mathbf{F}) \tag{3.6}$$

Projected along the axis of rotation it becomes

$$J\dot{\omega} = M + nNr\sin\varphi \tag{3.7}$$

Note that J is not constant if the web is deployed from the hub and out. First consider a point mass. Because stiffness and damping are not included, the equations of motion are simply

$$\mathbf{F} = m_c \ddot{\mathbf{R}} \tag{3.8}$$

Its position is obtained from Fig. 3.2 as

$$R = r + L \tag{3.9}$$

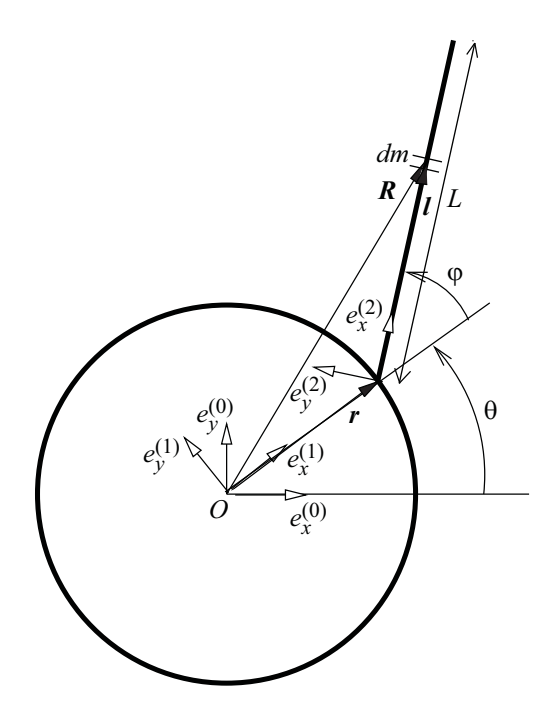


FIGURE 3.3. The analytical model for a distributed mass.

and the derivatives of \boldsymbol{R} become

$$\dot{\mathbf{R}} = \boldsymbol{\omega} \times \mathbf{r} + \mathbf{L}' + \left(\boldsymbol{\omega} + \dot{\varphi} \mathbf{e}_3^{(2)}\right) \times \mathbf{L}$$
(3.10)

$$\ddot{\mathbf{R}} = \dot{\boldsymbol{\omega}} \times \boldsymbol{r} + \boldsymbol{\omega} \times (\boldsymbol{\omega} \times \boldsymbol{r}) + \boldsymbol{L}'' + 2\left(\boldsymbol{\omega} + \dot{\varphi}\boldsymbol{e}_{3}^{(2)}\right)\boldsymbol{L}'$$

$$+ \left(\dot{\boldsymbol{\omega}} + \ddot{\varphi}\boldsymbol{e}_{3}^{(2)}\right) \times \boldsymbol{L} + \left(\boldsymbol{\omega} + \dot{\varphi}\boldsymbol{e}_{3}^{(2)}\right) \times \left(\left(\boldsymbol{\omega} + \dot{\varphi}\boldsymbol{e}_{3}^{(2)}\right) \times \boldsymbol{L}\right)$$
(3.11)

where ' denotes derivation in the local coordinate system ⁽²⁾. Projected and evaluated in the same coordinate system, the equations of motion become

$$\frac{m_c}{n} \left[r \left(\omega^2 \cos \varphi - \dot{\omega} \sin \varphi \right) - \ddot{L} + L \left(\omega + \dot{\varphi} \right)^2 \right] = N$$
 (3.12)

$$r\left(\dot{\omega}\cos\varphi + \omega^2\sin\varphi\right) + 2\dot{L}(\omega + \dot{\varphi}) + L\left(\dot{\omega} + \ddot{\varphi}\right) = 0 \tag{3.13}$$

where m_c is the total mass of all corner masses. Arms with distributed masses are described similarly. A small mass dm is at distance l, Fig. 3.3:

$$\mathbf{R} = \mathbf{r} + \mathbf{l} \tag{3.14}$$

 \ddot{R} can be computed as for a point mass but use of Eq. (3.14) instead of Eq. (3.9) in Eq. (3.11). The sum of the contributions from all small masses, $dm = \rho(l)dl$, is

$$\int_{0}^{L} \ddot{\mathbf{R}} \rho(l) dl \tag{3.15}$$

The mass per length, $\rho(l)$, is different for different folding patterns. For arms folded in star arms, $\rho(l)$ varies linearly, starting from zero at the tip of the arm. If the arm is deployed from the center hub and out, the mass per length of the deployed part is

$$\rho(l) = \frac{2m_w}{nL_{\text{max}}^2}(L - l) \qquad (0 \le l \le L)$$
(3.16)

The use of Eq. (3.16) in Eq. (3.15) yields:

$$\frac{2m_w}{nL_{\max}^2} \left[\frac{L^2}{2} \left(r \left(\omega^2 \cos \varphi - \dot{\omega} \sin \varphi \right) - \ddot{L} \right) + \frac{L^3}{6} \left(\omega + \dot{\varphi} \right)^2 \right] = N \tag{3.17}$$

$$\frac{L^2}{2}\left(r\left(\dot{\omega}\cos\varphi + \omega^2\sin\varphi\right) + 2\dot{L}(\omega + \dot{\varphi})\right) + \frac{L^3}{6}\left(\dot{\omega} + \ddot{\varphi}\right) = 0 \tag{3.18}$$

For an arm-folded space web with point masses in the corners, the equations of motion are added together, so that

$$a\left[r\left(\omega^{2}\cos\varphi - \dot{\omega}\sin\varphi\right) - \ddot{L}\right] + b\left(\omega + \dot{\varphi}\right)^{2} = nN$$
 (3.19)

$$a\left[r\left(\dot{\omega}\cos\varphi + \omega^2\sin\varphi\right) + 2\dot{L}\left(\omega + \dot{\varphi}\right)\right] + b\left(\dot{\omega} + \ddot{\varphi}\right) = 0 \tag{3.20}$$

where

$$a = a(L) = m_c + \frac{m_w L^2}{L_{\text{max}}^2}$$
 (3.21)

$$b = a(L) = L(m_c + \frac{m_w L^2}{3L_{\text{max}}^2})$$
 (3.22)

where $L_{\text{max}} = S/2 - \pi r/n$ and n was rearranged to the right hand side of Eq. (3.19). Different a and b can be used for different folding patterns and membrane geometries. For a split circular membrane [103] or its continuous equivalent, a hub-wrapped circular membrane [150], a and b become

$$a = a(L) = \frac{m_w L}{L_{\text{max}}^2} (2L_{\text{max}} - L)$$
 (3.23)

$$b = b(L) = \frac{m_w L^2}{L_{\text{max}}^2} \left(L_{\text{max}} - \frac{L}{3} \right)$$
 (3.24)

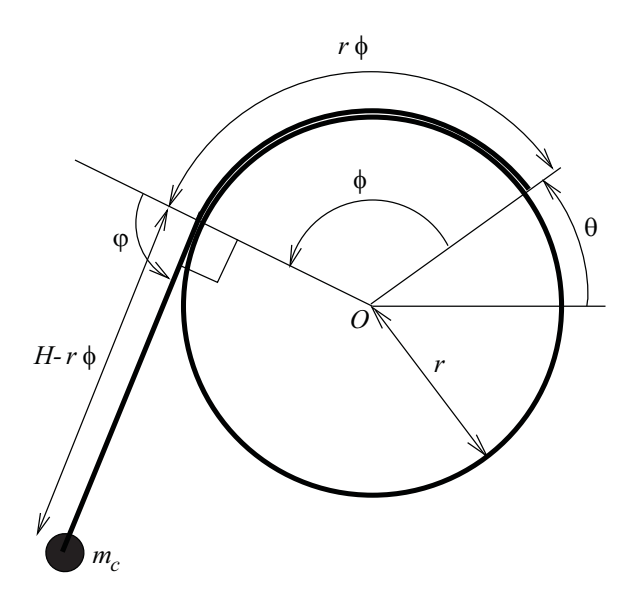


FIGURE 3.4. The analytical model for an arm coiled around the hub.

where $L_{\text{max}} = R - r$. Notice that this does not give a perfect circle, but close enough if $R \gg r$. For the LOFT [65]:

$$a = a(L) = m_c + m_t + \frac{2m_w L}{L_{\text{max}}^2} \left(L_{\text{max}} - \frac{L}{2} \right)$$

$$b = b(L) = L \left[m_c + \frac{m_t}{2} + \frac{m_w L}{L_{\text{max}}^2} \left(L_{\text{max}} - \frac{L}{3} \right) \right]$$
(3.25)

$$b = b(L) = L \left[m_c + \frac{m_t}{2} + \frac{m_w L}{L_{\text{max}}^2} \left(L_{\text{max}} - \frac{L}{3} \right) \right]$$
 (3.26)

where $L_{\text{max}} = R - r$. Evidently, Eqs. (3.12) and (3.13), with the appropriate expressions for a and b, can also be used for a point mass, where $m_w = m_t = 0$, or if there are no corner masses, i.e. $m_c = 0$. Similar expressions for the functions a and b can be obtained for different folding patterns [103, 150].

3.2.2. Equations for arms coiled around the hub. To simulate space webs that are coiled around the center hub, Fig. 3.3, first notice that $\varphi = \pm \pi/2$ (and $\dot{\varphi} = \ddot{\varphi} = 0$) when the arms are coiled around the hub. Then introduce the arm coiling angle, ϕ , which initially is equal to $\pm (L_{\text{max}}/r)$ for a completely coiled arm. When the arms are completely coiled off, Eqs. (3.19) and (3.20) can be used again, with $\varphi = \pm \pi/2$ at the transition. The current length of the coiled off part of the arm is

$$L = L_{\text{max}} - r|\phi| \tag{3.27}$$

and the angular velocity of the coiled off arm is

$$\omega_a = \omega + \dot{\phi} \tag{3.28}$$

It follows that $\dot{\omega}_a = \dot{\omega} + \ddot{\phi}$, $\dot{L} = -\text{sign}(\varphi)r\dot{\phi}$ and $\ddot{L} = -\text{sign}(\varphi)r\ddot{\phi}$. Finally, introduce $s_{\phi} = \text{sign}(\phi) = \text{sign}(\varphi)$, and the equations to solve for the coiled arms become

$$J\dot{\omega} = M + s_{\phi}nNr \tag{3.29}$$

$$-s_{\phi}ar\dot{\omega} + b\left(\omega + \dot{\phi}\right)^2 = nN \tag{3.30}$$

$$s_{\phi}ar\left(\omega^2 - \dot{\phi}^2\right) + b\left(\dot{\omega} + \ddot{\phi}\right) = 0 \tag{3.31}$$

where L in a and b are replaced with Eq. (3.27).

3.2.3. Dynamic constraints for arms coiled onto spools. If the membrane is deployed from spools on the tip of the arms, as in [103], or in separate parts from spools at the center hub, as in [65], then both N and M are used to control the deployment. The vector of state variables is

$$\mathbf{x} = (x_1, x_2, x_3, x_4, x_5)^T = (\omega, \varphi, \dot{\varphi}, L, \dot{L})^T$$
 (3.32)

and the vector of control variables is

$$\boldsymbol{u} = (u_1, u_2)^T = (M, nN)^T \tag{3.33}$$

and the governing equations can be written as a system of nonlinear ordinary differential equations:

$$\dot{x} = \begin{pmatrix} \dot{\omega} & \dot{\omega} \\ x_3 & \\ -\dot{\omega} - \frac{a}{b} \left[r \left(\dot{\omega} \cos x_2 + x_1^2 \sin x_2 \right) + 2x_5 (x_1 + x_3) \right] \\ x_5 & \\ r(x_1^2 \cos x_2 - \dot{\omega} \sin x_2) + \frac{b}{a} (x_1 + x_3)^2 - \frac{u_2}{a} \end{pmatrix}$$
(3.34)

where

$$\dot{\omega} = \frac{u_1 + ru_2 \sin x_2}{J} \tag{3.35}$$

3.2.4. Dynamic constraints for arms coiled around the hub. If the arms are coiled around the center hub only two DOFs, corresponding to three state variables, are required. The vector of state variables is

$$\boldsymbol{x} = (x_1, x_2, x_3)^T = (\omega, \alpha, \dot{\alpha})^T \tag{3.36}$$

where we have introduced the variable

$$\alpha = \phi + \varphi \tag{3.37}$$

because coiled arms become straight when they are completely coiled off. It is not possible to control the coiling off rate directly. Therefore, the vector of control variables is simply a scalar:

$$\boldsymbol{u} = u_1 = M \tag{3.38}$$

As shown in the previous sections, different equations are used to describe the deployment when the arms are partially coiled around the hub and when the arms are straight. If $|\alpha| < \pi/2$, i.e. the arms are straight, the system of ordinary differential equations to solve are derived from Eqs. (3.7), (3.12) and (3.13):

$$\dot{\boldsymbol{x}} = \begin{pmatrix} \dot{\omega} \\ x_3 \\ -\dot{\omega} - \frac{a}{b}r\left(\dot{\omega}\cos x_2 + x_1^2\sin x_2\right) \end{pmatrix}$$
(3.39)

where

$$\dot{\omega} = \frac{u_1 + r \sin x_2 \left(arx_1^2 \cos x_2 + b(x_1 + x_3)^2 \right)}{J + ar^2 \sin^2 x_2}$$
Instead, if $\alpha < -\pi/2$, i.e. the arms are coiled clockwise around the hub, then

$$\dot{\boldsymbol{x}} = \begin{pmatrix} \dot{\omega} \\ x_3 \\ -\dot{\omega} + \frac{a}{b}r\left(x_1^2 - x_3^2\right) \end{pmatrix} \tag{3.41}$$

where

$$\dot{\omega} = \frac{u_1 - br(x_1 + x_3)^2}{J + ar^2} \tag{3.42}$$

and L in a and b is given by

$$L = L_{\text{max}} + r(x_2 + \frac{\pi}{2}) \tag{3.43}$$

Finally, if $\alpha > \pi/2$, i.e. the arms are coiled counter-clockwise, the differential equations are obtained analogously as for $\alpha < \pi/2$ from Eqs. (3.29)–(3.31).

3.3. Optimal control

3.3.1. Optimal control methods. Optimal control problems can be solved by either indirect or direct methods [14]. Indirect methods derive analytical expressions for the costates from the necessary optimality conditions given by Pontryagins maximum principle [131]. Contrary to many other practical problems, for this problem it is possible to obtain the necessary optimality conditions, but the result is a multipoint boundary value problem (MBVP) that is more complicated to solve than the original problem. The reasons are: (i) twice as many unknowns, and thus differential equations, are required, because each state corresponds to a costate, and (ii) good initial guesses are required to solve the MBVP numerically, because the region of convergence is small, but initial values for the costates are difficult to obtain.

Contrary, direct methods directly discretize the continuous-time optimal control problem and transcribe it into a parameter optimization problem, that can be solved

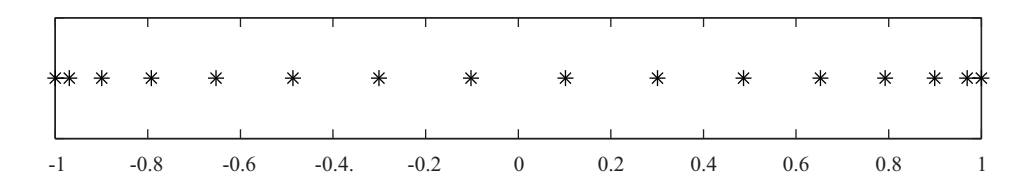


FIGURE 3.5. The Legendre–Gauss–Lobatto points.

using standard nonlinear programming (NLP) tools [24]. The parameters for the NLP are either the values of the control, or more commonly, both the control and the states at carefully selected collocation points. Direct transcription of optimal control problems requires approximations of the integration in the cost function, the differential equations of the state-control system, and the state-control constraint equations, and ideally the same collocation points are used for all. In principle any set of unique collocation points and any discretization methodology can be used. One possibility is to use local piecewise-continuous approximations for the differential equations, e.g. Hermite-Simpson [62] and Runge-Kutta [29], combined with e.g. Gauss quadrature to integrate the cost function. A better option is to use pseudospectral (PS) methods because they converge with spectral accuracy for smooth problems [151]. PS methods are efficient for all the three approximations as proved in [56, 57, 77]. All PS methods use an orthogonal polynomial of degree N evaluated at N+1 points. The points are usually the N-1 roots of the polynomial and the boundaries of the domain [-1,1]. Exact integration for a polynomial of degree N is obtained for this set of points. The use of many different orthogonal polynomials have been investigated, e.g. Legendre [32, 34, 56, 57, 77], Chebyshev [35, 157] and Jacobi [159], Radau [33] or Gauss [12] polynomials.

The Legendre PS method is the most widely used PS method because of its proven convergence properties, which makes it possible to accept or reject solutions based on the optimality conditions [56,57,77]. Lagrange interpolation polynomials, based on the Legendre polynomial of degree N, are used to create trial functions that connect the discrete and the continuous state and control variables. The Legendre–Gauss–Lobatto points are used as collocation points. The Gauss–Lobatto quadrature rule is used for the integration of the objective function. This method is available in the Matlab-based commercial code DIDO [135]. A free version also exist for a limited number of DOF. However, here the problem was solved directly in Comsol script [23] since the implementation of the algorithms is rather straightforward. The collocation points and the values of the Legendre polynomials in these points were calculated in Maple [92] because double precision with 16 digits, which is the highest precision in Matlab [149] and Comsol, is insufficient if many collocation points are required. Finally, the NLP problem was solved using the SNOPT [51]-based Comsol Optimization Lab [22].

3.3.2. Legendre pseudospectral method. The Legendre pseudospectral method is a direct transcription method that transforms an optimal control problem into an NLP problem. First, note that a general optimal control problem is to minimize the Bolza cost function

$$\min_{\boldsymbol{u}} J(\boldsymbol{x}(t), \boldsymbol{u}(t), t) = \int_{t_0}^{t_f} F(\boldsymbol{x}(t), \boldsymbol{u}(t), t) dt + G(\boldsymbol{x}(t_0), t_0, \boldsymbol{x}(t_f), t_f)$$
(3.44)

subject to some dynamic constraints

$$\frac{d\mathbf{x}}{dt} = \mathbf{f}(\mathbf{x}(t), \mathbf{u}(t), t) \tag{3.45}$$

and boundary conditions

$$\boldsymbol{g}(\boldsymbol{x}(t_0), t_0, \boldsymbol{x}(t_f), t_f) \le \mathbf{0} \tag{3.46}$$

and inequality path constraints

$$h(x(t), u(t), t) \le 0 \tag{3.47}$$

The aim of this section is to approximate the integral in Eq. (3.44) and to discretize the dynamic constraints in Eq. (3.45). For all PS methods, the original problem is first transformed from the original time domain $t \in [t_0, t_f]$ to the time domain on which the orthogonal polynomial is defined $\tau \in [\tau_0, \tau_N] = [-1, 1]$ by the transformation

$$t = \frac{[(t_f - t_0)\tau + (t_f + t_0)]}{2}$$
(3.48)

It follows that

$$\frac{d\mathbf{x}}{dt} = \frac{1}{\psi} \frac{d\mathbf{x}}{d\tau} = \mathbf{f}(\mathbf{x}(\tau), \mathbf{u}(\tau), t(\tau))$$
(3.49)

and

$$\int_{t_0}^{t_f} F(\boldsymbol{x}(t), \boldsymbol{u}(t), t) = \psi \int_{-1}^{1} F(\boldsymbol{x}(\tau), \boldsymbol{u}(\tau), t(\tau)) d\tau$$
 (3.50)

where

$$\psi = \frac{t_f - t_0}{2} \tag{3.51}$$

If the state and control constraints in Eqs. (3.46) or (3.47) in rare cases include derivatives, then the same procedure is used for them. The second step is to define the discretizing trial functions and the collocation points. Let $L_N(\tau)$ be the Legendre polynomial of degree N on the interval [-1,1]. Then define the vector of continuous state and control variables

$$y(\tau) = \begin{pmatrix} x(\tau) \\ u(\tau) \end{pmatrix} \tag{3.52}$$

Each state and control variable, $y(\tau)$ can be approximated, with Lagrange interpolating polynomials of degree N as trial functions, according to

$$y^{N}(\tau) = \sum_{i=0}^{N} \phi_{i}(\tau)y_{i}$$
 (3.53)

where

$$\phi_i(\tau) = \frac{1}{N(N+1)L_N(\tau_i)} \frac{(\tau^2 - 1)\dot{L}_N(\tau)}{\tau - \tau_i}$$
(3.54)

and the unknowns

$$y_i = y(\tau_i) \tag{3.55}$$

are the state and control variables in the N+1 Legendre-Gauss-Lobatto points, Fig. 3.5. The derivative $\dot{y}^N(\tau)$ can be expressed in terms of the y_i s by differentiation of Eq. (3.54). Evaluated at the collocation points t_i it is obtained that

$$\frac{\partial y^N(\tau_i)}{\partial \tau} = \sum_{j=0}^N D_{ij} y_j \tag{3.56}$$

where the elements D_{ij} are

$$D_{ij} = \begin{cases} \frac{L_N(\tau_j)}{L_N(\tau_i)} \frac{1}{\tau_j - \tau_i} & j \neq i \\ -\frac{N(N+1)}{4} & j = i = 0 \\ \frac{N(N+1)}{4} & j = i = N \\ 0 & \text{otherwise} \end{cases}$$
(3.57)

For each state x_k , the derivative in Eq. (3.45) is replaced with the expression in Eq. (3.56) to obtain a set of N constraint equations

$$\frac{1}{\psi} \sum_{j=0}^{N} D_{ij} x_j - f_k(\boldsymbol{x}_i, \boldsymbol{u}_i, \tau_i) = 0 , i = 0, ..., N$$
 (3.58)

In total, Eq.

(3.45) is discretized into $M \times (N+1)$ constraints for M state variables and N+1 collocation points. The integral part in the objective function is evaluated using the Gauss-Lobatto quadrature rule

$$\int_{t_0}^{t_f} F(\boldsymbol{x}(t), \boldsymbol{u}(t), t) \approx \psi \sum_{i=0}^{N} w_i F(\boldsymbol{x}(\tau_i), \boldsymbol{u}(\tau_i), t(\tau_i))$$
(3.59)

where the weights are

$$w_i = \frac{2}{N(N+1)(L_N(\tau_i))^2}$$
(3.60)

3.3.3. Sequential Quadratic Programming. Comsol Optimization Lab [22] is used to solve standard NLP problems. It is based on the SNOPT solver [52], which uses a sparse sequential quadratic programming (SQP) method, with SQOPT [53] as the quadratic programming (QP) subproblem solver. An NLP problem has a nonlinear objective function, nonlinear constraints, or both, and is defined as

$$\min J(\boldsymbol{y}) \tag{3.61}$$

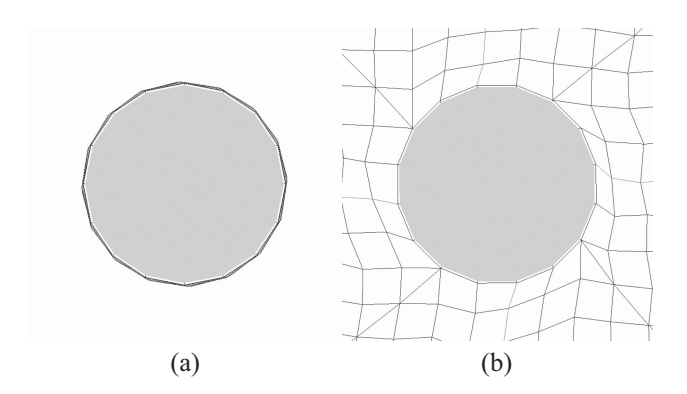


FIGURE 3.6. The hub-web at the initial (a) and final (b) stages.

subject to

$$\boldsymbol{b}_{lb} \le \mathbf{A}\boldsymbol{y} \le \boldsymbol{b}_{ub} \tag{3.62}$$

$$d_{lb} \le c(y) \le b_{ub} \tag{3.63}$$

$$\boldsymbol{y}_{lb} \le \boldsymbol{y} \le \boldsymbol{y}_{ub} \tag{3.64}$$

y is a vector with all variables, J(y) is the cost function or objective function, \mathbf{A} defines the linear constraints together with the lower bounds, b_{lb} , and the upper bounds, b_{ub} . c(y) defines the nonlinear constraints together with the lower bounds, d_{lb} , and the upper bounds, d_{ub} . y_{lb} and y_{ub} define the lower and upper bounds for the variables y. Equality constraints are defined by setting the upper and lower bounds for the inequality constraints equal.

Translated from the optimal control problem, \mathbf{y} is a vector with all state and control variables in all collocation points. The discretized dynamical constraints in Eq. (3.58) goes into the nonlinear constraints, Eq. (3.63). The path constraints in Eq. (3.47) goes into Eq. (3.64). The boundary conditions in Eq. (3.46) often fits in the linear constraints, Eq. (3.62), where \mathbf{A} is a sparse matrix, with 1 for all entries that are on the diagonal and corresponds to $\mathbf{x}(t_0)$ or $\mathbf{x}(t_0)$ and 0 elsewhere. The SQP solver solves a series of QP problems. At each iteration, the original nonlinear optimization problem is locally modeled as a quadratic objective function with linear constraints. Starting at a feasible point, i.e. a point that satisfies all constraints, the algorithm, that is based on the method of steepest descent, iteratively moves the solution vector in the direction of the gradient of the objective function,

3.4. Finite element model

3.4.1. Overview. A three-dimensional FE model including the center hub, the web and four corner masses was implemented. However, the center hub was

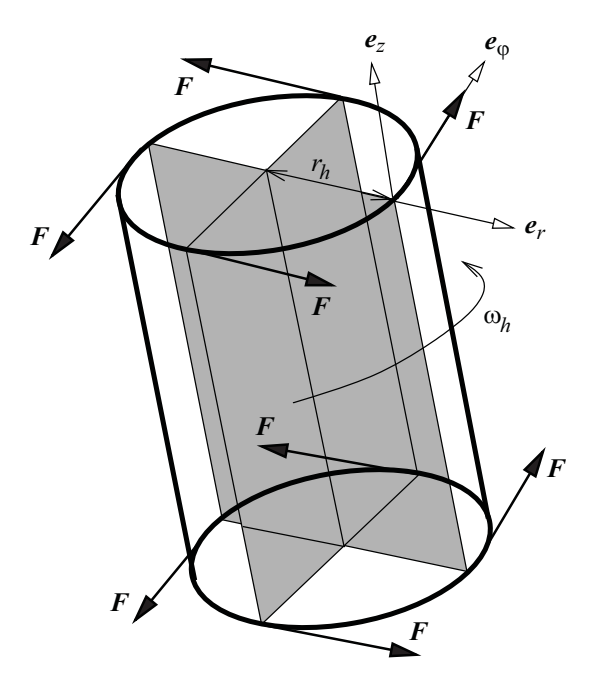


FIGURE 3.7. Torque applied as forces on extra shells in the FE model.

constrained to move around its center axis, thus the center hub motion was two-dimensional. The node and element geometry and connectivity were generated in Matlab [149]. The equations of motion were then solved in LS-DYNA [85] using the central difference method for explicit time integration.

The main differences compared to the analytical model are that other deployment sequences than arm deployment can be studied with the FE model, the arms are not necessarily straight during the deployment, the cables can store elastic energy and perturbations can be studied. The gravity gradient and energy dissipation can be included, but have been considered small for membranes in comparison with the rotational inertia forces [103], and should be even smaller for a web. Effects of the hub orbit and hub direction in orbit are interesting, as discussed in [127], but was not a topic of the present study.

The progression of a spin deployment is highly dependent on the folded configuration. Besides of providing the initial geometry, several other problem characteristics are also due to the folding: (i) the initial velocities of all parts are proportional to their distances to the rotation axis, i.e. the initial conditions depend on the folding; (ii) the forces between the center hub and the web during the deployment depend strongly on the current web formation and the current tension in the web, i.e. the forces applied to the web depend on the folding; (iii) the boundary conditions depend, in some sense, on the folding since some parts of the web constrain others from moving. As a consequence, the accuracy of a FE model is strongly dependent on how well the modeled folded configuration coincides with the real one. In some respects, the modeled configuration may be too perfect, and in other respects, the computational cost puts limitations on the model. Nevertheless, since it is difficult to analytically predict the deployment of a web or membrane, the FE model serves as a valuable second analysis step after the analytical arm deployment model.

In reality, the mesh width of the web would be at most 30 mm and the amplitude of swaying motions would be very small. In the FE model, a significantly larger mesh width, 2.5 m, was used for computational efficiency. Having a single truss element between two nodes disregards the lateral inertia of the cable, so multiple truss or beam elements are often used in dynamic analyzes. Here, only one truss element was used to connect two nodes, because dividing the cable into more truss elements would allow in-plane swaying motions that would not be present in reality. It is proposed [75] that cables are best modeled with truss elements and a material with no-compression properties to model cable slackening under compressive loads. Therefore, the cables were here modeled as truss elements with pin-jointed ends. This truss element is based on a co-rotational formulation and the internal force for the no-compression material is computed as [60]:

$$N_{ca} = \max(E_{ca}A_{ca}\varepsilon, 0) \tag{3.65}$$

Formulation (3.65) does not take into account the changes of volume and cross-sectional area, which were considered negligible in this case because of small strains.

The proposed folding scheme assumes that the cables can be bent only at the nodes and that the distance between the fold lines is twice the mesh width. These choices mean that the radius of the hub, which fits in the central deployed part of the web, Fig. 3.6(b), is dependent on the mesh width. Thus, for a coarse web, the hub radius is unrealistically large, but still adequate for evaluating the spin deployment of the space web. This artificial constraint on the hub size is difficult to overcome, since a certain number of web elements must be attached to the center hub to accurately transfer the angular momentum from the center hub to the web. The governing equations of the folding scheme are given in Ref. [150].

The center hub was modeled as a cylinder with rigid material. It was divided into 16 identical pentahedrons to achieve the cylindrical shape. However, this did not increase the computational cost for the dynamical analysis since the hub was constrained to move as a rigid body. In the corners, point masses were considered sufficiently accurate, because the contact between them and the web was not considered important. The contact between the cables and the rigid center hub was modeled using the kinematic constraint method [68]. This contact is completely

inelastic and the contact assumption implies that cables in contact with the hub follow the hub. It is not obvious how to coil the web near the hub and include initial contact. Therefore, contact between cable elements in the space web were disregarded, since higher priority was given to the coiling of the space web as close to the center hub as possible, Fig. 3.6(a).

The control torque depends on the angular velocity of the center hub, and since the angular velocity varies with time, the control cannot be specified without special treatment in FE softwares. In the object version of LS-DYNA, the user can implement in the source code a function that applies a force to shell or beam elements [2]. The user predetermines some parameters for this function, and at each timestep, the program supplies values of e.g. the position, velocity and accelerations of the nodes in the element. Therefore, to apply the torque, four planar shells with negligible mass were symmetrically positioned in the center hub, Fig. 3.7. Four shells were chosen to distribute the small mass evenly and because the velocity of the center is required. The nodes of each shell were put at the top and bottom of the center hub, two at the axis of rotation and two at the periphery at the same point as the center of the arms. From the control moment in Eq. (4.1), the forces on the nodes on the shells can be calculated as

$$F = \frac{\widehat{M}}{pr} \left(1 - \frac{\omega}{\omega_0} \right) \tag{3.66}$$

Here, eight peripherical nodes were used. \widehat{M} , ω_0 , r and p were defined as user parameters. The angular velocity was calculated from the velocities and positions of the two nodes at the rotation axis and one of the peripherical nodes. First a local cylindrical coordinate system (e_r, e_{φ}, e_z) was set up. Then ω was determined from

$$v_{\varphi} \boldsymbol{e}_{\varphi} = \omega \boldsymbol{e}_z \times r \boldsymbol{e}_r \tag{3.67}$$

 v_{φ} is the velocity of the peripherical node, relative to the corresponding node on the rotation axis, projected along e_{φ} .

- **3.4.2.** Web folding. Note that the parameters in this section are not included in the nomenclature list.
- 3.4.2.1. Complete star pattern. The first step of the folding is to fold the web into a 'star'-like shape. The y-coordinate of a node on the centre line is described as

$$y = y_0 \sin \frac{\theta}{2} \tag{3.68}$$

where θ is the fold angle along the centre line ($\theta = 180^{\circ}$ for a fully deployed configuration and 0° when completely folded) and y_0 is the y-coordinate of the node in the deployed configuration. Equation (3.68) is the mapping scheme of the

nodes along the centre line. For a node i in the first and second quadrants and lying between the side lines the mapping scheme is

$$x_i = x_{0i}\cos\phi \tag{3.69}$$

$$y_i = y_{0i} \sin \frac{\theta}{2} + |x_{0i}| \sin \phi \tag{3.70}$$

where

$$\phi = \arccos\left(\frac{\sin\frac{\theta}{2}\cot\frac{\pi}{n} + \sqrt{\tan^2\frac{\pi}{n} + \cos^2\frac{\theta}{2}}}{\tan\frac{\pi}{n}\left(1 + \cot^2\frac{\pi}{n}\right)}\right)$$
(3.71)

Equations (3.69) and (3.70) describe the movement of a node in the x-y plane during the 'star' folding process. Evidently, the movement of the fold lines, from the fully deployed to the fully folded configurations, is not linear.

Since the surface in the z-direction has a zig-zag pattern, the mapping for the z-coordinate is a bit more complex. Assuming that the distance between fold lines is 2Δ in the interior and Δ at the centre and along the edges, the relative position of the node between two fold lines is computed as

$$\chi = y_{0i}/2\Delta - \lfloor y_{0i}/2\Delta \rfloor \tag{3.72}$$

where $\lfloor x \rfloor$ rounds x to the nearest integer towards $-\infty$. The mapping scheme for the z-coordinate becomes

$$z_{i} = \begin{cases} \pm 2\chi \Delta \cos \frac{\theta}{2} & \text{if } \chi \leq 0.5\\ \pm 2(1-\chi)\Delta \cos \frac{\theta}{2} & \text{if } \chi > 0.5 \end{cases}$$
(3.73)

where the '-' sign holds if $|y_{0i}/2\Delta|$ is an even number and the '+' sign otherwise.

In summary, the star pattern is neatly described by analytical relationships which maps the coordinates from a given position of the deployed configuration to a position of the folded configuration described by the single variable θ . In this way, the curved edges of the web can be mapped to the folding pattern even though the edge nodes do not lie on the fold lines.

3.4.2.2. Incomplete star pattern. If the central satellite is modelled as a point mass with inertia, the complete star mapping scheme, which folds the web towards the centre point, can be used. If, however, the central satellite is modelled with shell elements and its physical dimensions, the complete star mapping cannot be used. In such a case, the star mapping must be modified to have the two innermost rings of elements deployed. The starting configuration for this scheme is the star folding with folding angle $\theta = 0^{\circ}$ (all nodes of the arms are positioned along straight lines). From this position, the two inner rings of elements are deployed. Note that the incomplete star mapping only works for a fold angle $\theta = 0$, since the arms

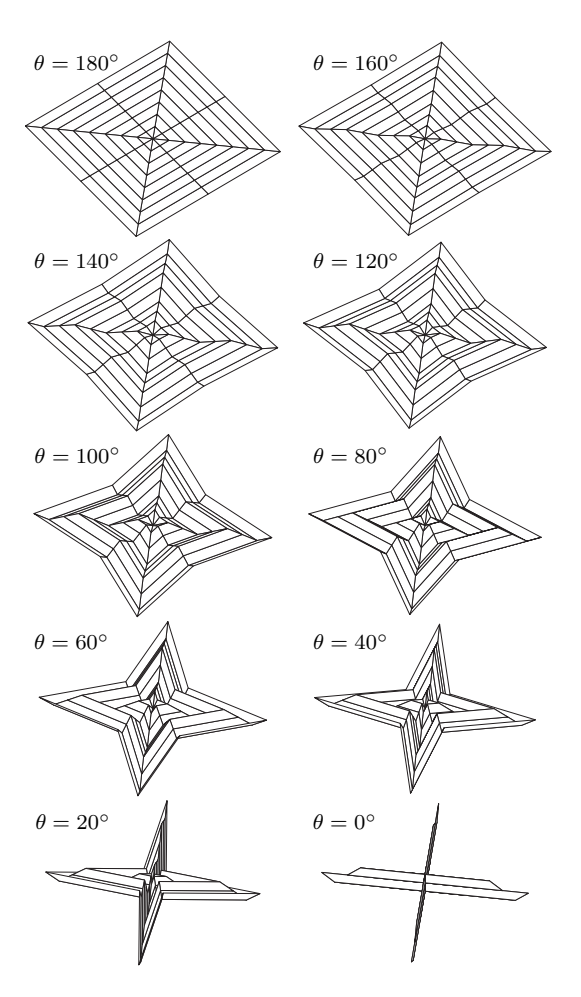


FIGURE 3.8. Complete star folding sequence for a quadratic sheet (note that all lines are not fold lines).

have to be completely folded before the two innermost rings can be deployed. The incomplete star mapping scheme is written as

$$x_{i} = \begin{cases} x_{0i}\cos\phi + 2\Delta \operatorname{sgn}(x_{0i})\tan\frac{\pi}{n}\left(1 - \sin\frac{\pi}{n}\right) & \text{if} \quad |x_{0i}| > 2\Delta \tan\frac{\pi}{n}; \ y_{0i} > 2\Delta \\ x_{0i} & \text{if} \quad |x_{0i}| \le 2\Delta \tan\frac{\pi}{n} \end{cases}$$
(3.74)

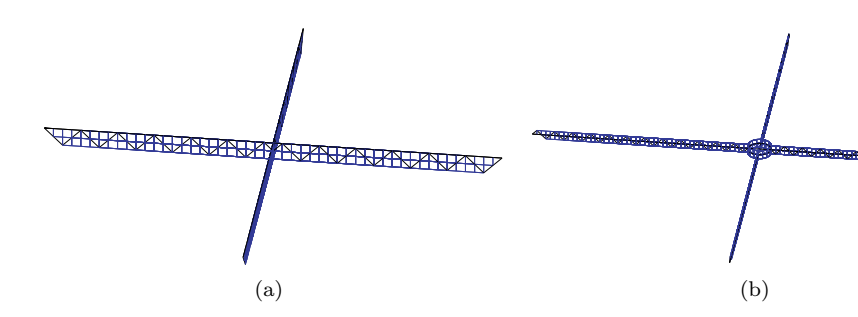


FIGURE 3.9. Visual comparison of the (a) complete and (b) incomplete star patterns.

and

$$y_{i} = \begin{cases} y_{0i} \sin \frac{\theta}{2} + |x_{0i}| \sin \phi + 2\Delta \tan \frac{\pi}{n} \left(1 - \cos \frac{\pi}{n}\right) & \text{if } |x_{0i}| > 2\Delta \tan \frac{\pi}{n}; y_{0i} > 2\Delta \\ 2\Delta & \text{if } |x_{0i}| \le 2\Delta \tan \frac{\pi}{n}; y_{0i} \ge 2\Delta \\ y_{0i} & \text{if } y_{0i} < 2\Delta \end{cases}$$

The z-coordinates are basically unchanged, except for the nodes lying within the first two element rings defined by the y-coordinate:

$$z_i = \begin{cases} \text{Eq. (3.73)} & \text{if } y_{0i} \ge 2\Delta \\ 0 & \text{if } y_{0i} < 2\Delta \end{cases}$$

$$(3.76)$$

A comparison between the complete and incomplete star mapping schemes is shown in Figure 3.9. In order to facilitate a tight wrapping around the hub, the square deployed part of the web is made circular while preserving the length of all elements. This last change is very important since it otherwise will be a significant space between the coiled web and the surface of the cylindrical hub.

A disadvantage with the proposed incomplete star pattern is that the size of the deployed inner portion of the web is dependent on the mesh size of the web, which may produces an unrealistically large radius of the stowed package. However, a general folding routine, where the fold lines do not have to coincide with the nodal lines, was deemed too complicated and costly to implement for the present project.

3.4.2.3. Coiling of star arms. A folding scheme that is attractive due to its simplicity is the wrap-around or coiling scheme, where the star arms are coiled around the central satellite. It is important for this scheme that the folding is done in a polygonal way and not by a smooth curve since the fold lines must be positioned where the nodes are. Otherwise, the elements will be modelled too short for the web to deploy properly. A mapping scheme, which preserves the lengths

of all members can be written using the Denavit–Hartenberg convention, [28]. As the movement of the nodes during the folding only is in one plane, the Denavit–Hartenberg transformation matrix can be simplified to

$$\mathbf{A}(\alpha) = \begin{bmatrix} \cos \alpha & -\sin \alpha & 0 & \Delta_w \cos \alpha \\ \sin \alpha & \cos \alpha & 0 & \Delta_w \sin \alpha \\ 0 & 0 & 1 & 0 \\ 0 & 0 & 0 & 1 \end{bmatrix}$$
(3.77)

where Δ_w is the distance between the fold lines or mesh width, α_i is the rotation angle relative to the previous segment of the star arm. For the first element, the folding angle is set to $\beta + \alpha_i/2 - \pi/2$ as the whole star arm first must be folded 90° from its initial angle β

$$\beta = \begin{cases} \arcsin \frac{y_i}{r_i} & \text{if } \frac{x_i}{r_i} \ge 0\\ \pi - \arcsin \frac{y_i}{r_i} & \text{if } \frac{x_i}{r_i} < 0 \end{cases}$$
(3.78)

where r_i is

$$r_i = \sqrt{x_i^2 + y_i^2} (3.79)$$

The folding of the star arms with $\alpha = 0$ is shown in Figure 3.10(a). To produce a circle of the star arms that encloses the deployed portion of the web, the following value for the relative rotation of the star arm segment must be chosen:

$$\alpha = -\left[\pi - 2\arccos\left(\frac{\Delta_w}{2\sqrt{r_0^2 + \frac{\Delta_w^2}{4}}}\right)\right] \tag{3.80}$$

The x- and y-coordinates of the position of the first node of the star arm $(r_1 = r_0 + \Delta_w)$ after folding is found as elements (1,4) and (2,4), respectively, in $\mathbf{A}(\beta - \pi/2 + \alpha/2)$. Similarly, the position of node i is found as positions (1,4) and (2,4) in the resulting matrix from the product $\mathbf{A}(\beta - \pi/2 + \alpha/2)\mathbf{A}(\alpha)^{i-1}$. Applying the Denavit–Hartenberg transformation for all nodes of the star arms yields the folded configuration in Figure 3.10(b). Since the star arms in this position lie on top of each other, problems might arise in the finite element simulations. Therefore, a slight change in the relative rotation angle α is implemented: for node i the relative rotation is set to

$$\alpha_i := \alpha - (i - 1)\vartheta \tag{3.81}$$

where ϑ is chosen as a fraction of α . It is found that $\vartheta = 0.01\alpha$ yields enough separation between the star arms, Figure 3.10(c). Hence, the x- and y-coordinates for node i is now found at positions (1,4) and (2,4) in the matrix $\mathbf{A}(\beta - \pi/2 + \alpha/2)\mathbf{A}(\alpha_1)...\mathbf{A}(\alpha_{i-1})\mathbf{A}(\alpha_i)$, where α_i is given by Eq. (3.81).

Zig-zag folding of the star arms could also be used if both the deployment rate and the torque to the hub are used for control. Zig-zag folding is described in [150].

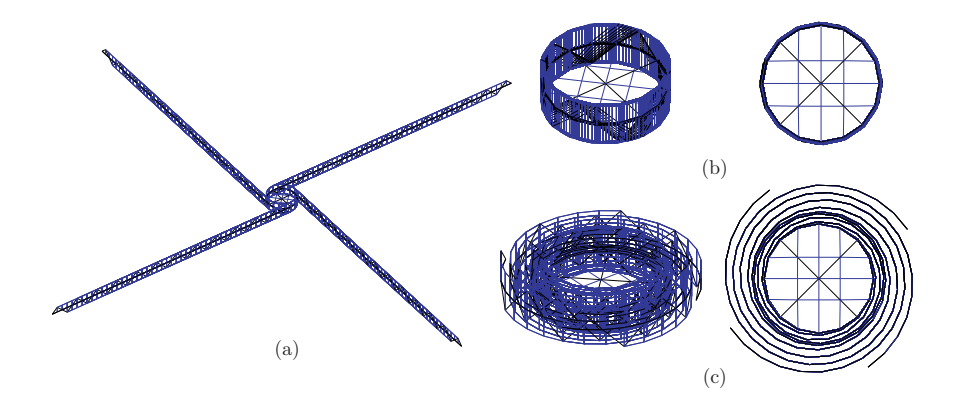


FIGURE 3.10. Hub-wrapping folding of the star arms: (a) initial 90° folding, (b) most compact folding with square (aerial and top views), and (c) with separation between the arms.

3.5. Elements for membrane modelling

3.5.1. Background. Deployment simulations of inflatable structures, e.g. car airbags, are usually performed with membrane finite elements, i.e. the bending stiffness is neglected. For space inflatables even a vanishingly small bending stiffness may have non-negligible effects. In the micro-gravity environment of space, the strain energy induced by the folding of the structure, may be sufficient to cause premature deployment for certain structures, e.g. crease-pattern folded tubes [136]. Wrinkling is also an important issue in many applications. Therefore, it is crucial to take into account the bending stiffness, and shell elements should thus be used.

3.5.2. Shell elements. It is not possible to summarize all research devoted to the analysis of plate and shell structures in this short introduction. An extensive review of this topic is written by Yang *et al.* [163], who categorize the shell elements into nine groups. However, here it is enough to divide them into three different categories, as in [25]:

- Flat elements, formed by combining a membrane element and a plate element.
- Degenerated solid elements, formed from three-dimensional elements.
- Curved elements based on classical shell theory.

The two first are the most commonly used. The merits of the first are: simplicity, acceptable performance, and compatibility to standard beam elements. The second approach is better for curved shell geometries and the performance is good, but

special methods must be used to avoid locking problems. In the analysis of non-linear problems, particularly transient non-linear problems such as the deployment of flexible structures, element stiffness computations are repeated many times and it is advantageous to have efficient and simple elements. Therefore, the first element type is considered in this thesis.

The next choice is between triangular and quadrilateral elements. Triangular elements are easier than quadrilaterals to fit to arbitrary geometries. Because of this, many computer aided design (CAD) packages include mesh generators which use triangular elements in their discretisation. Automatic mesh refinement algorithms are also usually based on triangular element discretisation. Furthermore, triangular shell elements are not subject to zero energy modes inherent in quadrilateral element formulations. Therefore, triangular elements are preferred in this study.

Three-noded triangles usually have 9 DOFs (w, θ_x and θ_y at each node), whereas a complete polynomial of third order has 10 unknown coefficients. Different techniques must be used to overcome this problem. Bazeley et~al. [9] eliminated the tenth DOF in such a way that completeness was obtained. However, even though it only converged for certain meshes, variants of it are still used.

An interesting study of flat three-noded plate bending finite elements with nine DOF was presented by Batoz et al. [8], who concluded that the discrete Kirchhoff theory (DKT) is the most reliable and efficient in its category of elements. The DKT plate element was compared to (i) elements using Mindlin–Reissner theory and selectively reduced integration, employed by e.g. Belytschko et al. [10], and (ii) a hybrid stress model, employed by e.g. Razzaque [132]. The DKT plate element can be combined with variants of the Allman triangle [4] to form the element denoted DKT18, a three-noded triangle with six DOFs per node.

An even simpler plate bending element was developed by Morley [111] who used only six DOFs, the three transversal displacements, w, and the rotations around the edges, θ_n , to compute constant curvatures normal to the edges. Batoz *et al.* [134] and Peng and Crisfield [128] combined Morley's element [111] with a constant strain triangle (CST) [155] to form shell elements with twelve DOFs.

3.5.3. Rotation-free shell elements. Even more simple and rapidly computed shell elements can be derived. RF shell elements is a family of shell elements that uses only the transversal displacements of a patch of four elements to approximate the curvatures of the mid element, Figure 3.11. For a plate bending element only one DOF, w, per node is required. For a shell element the three nodal displacements are used, i.e. no additional nodes are required compared to the membrane element.

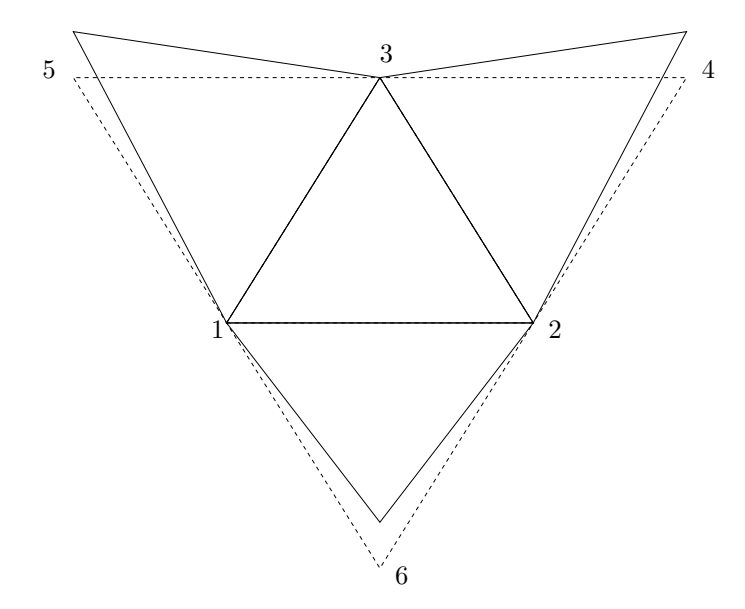


FIGURE 3.11. A patch of elements used to compute the bending behaviour of a rotation-free shell element.

The works by Barnes [7], Chan and Davies [19], Hampshire et al. [61], Sabourin and Brunet [15,137] and Guo et al. [59] resulted in an RF shell element that, compared to the element by Morley [111], approximates the rotation around each edge from the displacements of the four nodes of the two elements sharing the edge. Constant curvatures are then obtained around each edge, and superposition of the contributions is used to approximate constant curvatures over the patch.

Phaal and Calladine [129] used a complete quadratic polynomial in two dimensions to assume constant curvatures over the whole patch of elements. Their plate element was refined to enable computation of the curvatures for initially non-coplanar element patches, and combined with the CST, to form a shell element [130]. In paper 4 [47], it was shown that this formulation is particularly interesting for unstructured meshes, where many other RF elements show bad accuracy.

A third approach was used by Oñate and Cervera [123], who used integration by parts of the curvatures to derive their plate bending element. The deflection gradients are then employed directly, but a relationship to obtain constant curvatures over the patch or the edge does not exist. Oñate et al. also published formulations of this element for the analysis of shells [125], large deformations [122] and kinked and branched shells [38]. Flores and Oñate [37,124] have also proposed to use overlapping isoparametric linear strain triangles (LST) to describe the membrane behaviour.

Other, completely different RF formulations do exist. Cirak et al. [21] use subdivision surfaces, which are extended to large deflections [20]. Rio et al. [84] develop a shell element which takes into account both large displacements and coupling effects between membrane and bending behaviour. This element uses isoparametric interpolation in an attempt to model constant curvatures normal to each edge, which leads to problems in finding suitable integration points. Hauptmann and Schweizerhof [63] have developed an RF element degenerated from solid elements, where the displacements of the top and bottom surfaces are required. Recently Dung and Wells [30] presented a general formulation for geometrically nonlinear RF elements based on Lagrange basis functions. RF elements have also been developed for quadrilateral elements [16, 36].

3.5.4. Test problems. To enable comparison between different finite element formulations standard test problems are required. The obstacle course for shell elements by Belytschko *et al.* [11] is widely employed. It contains three test problems: the Scordelis-Lo roof, the Hemispherical shell and the Pinched cylinder. This obstacle course was inspired by the finite element standard set of problems by McNeal and Harder [86], who used the first two examples. A more challenging test problem for shells is the Raasch Hook [80]. All of these examples are described and used to test the performance of the RF shell elements in paper 4.

Results

4.1. Summary of the most important results from papers 1-3

The fundamental laws of conservation of angular momentum and conservation of energy yield that torque-free centrifugal force deployment of very large expandable structures would result in a very low final angular velocity for the deployed structure and most of the initial kinetic energy must be removed somehow. Furthermore, several studies, e.g. Refs. [13, 106, 150], indicate that an uncontrolled web would coil off and onto the hub repeatedly like a yo-yo. This is also shown in paper 1 and 2 for a quadratic space web, using both the analytical and the FE model, Fig. 4.1. Bergamin and Izzo [13] examine if only deployment length control can be used, and demonstrate analytically that such deployment is uncontrollable, at least in a linear case near $\alpha=0$. Thus, a torque must be applied.

Inspiration was found from the only successful spin deployment of a large structure in space, the deployment of the Russian Znamya-2 membrane reflector in 1993. A simple control strategy was proposed for the Znamya-2 deployment by Melnikov

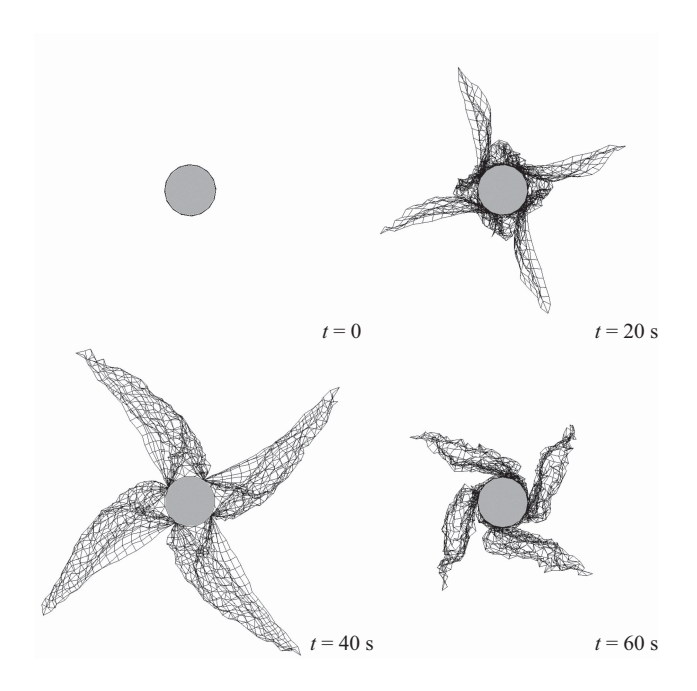


Figure 4.1. Uncontrolled deployment of arms.

40 4. RESULTS

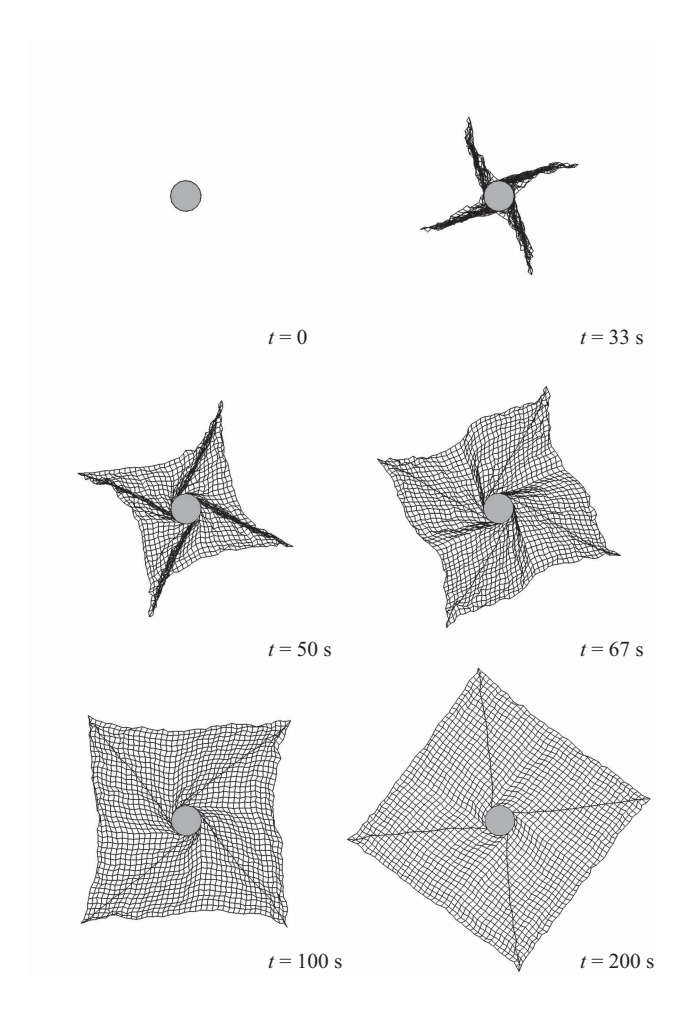


FIGURE 4.2. Controlled one-step deployment of space web.

and Koshelev [103]. The split membrane mirror was folded in star arms, and the arms were coiled on spools. The deployment occurred in two separate steps: first the arms were coiled off, then the whole membrane was tether-controlled. In both phases, the deployment velocity was constant and the torque was given by a feedback law with drooping characteristics:

$$M = \widehat{M} \left(1 - \frac{\omega}{\omega_0} \right) \tag{4.1}$$

where M is the applied torque, \widehat{M} is a constant that can be interpretated as an upper bound for the torque, ω is the angular velocity of the center hub and 0 denotes the initial state. This control law is henceforth denoted the MK-law.

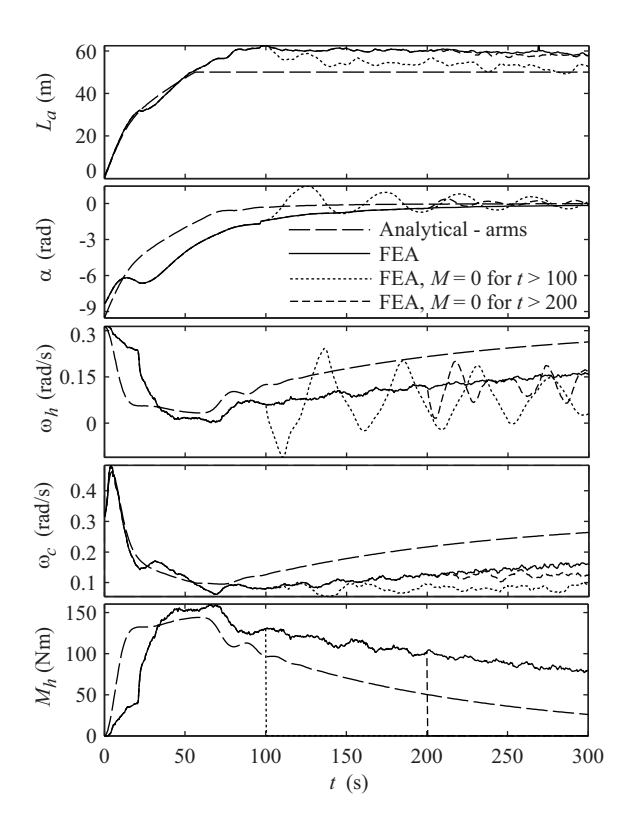


FIGURE 4.3. Controlled one-step deployment of space web.

A quadratic space web can be folded similarly, as described in the report [150] that paper 1 is a summary of. An important difference is that a web, with moving spider robots, cannot be split into several sheets. The natural folding is therefore to coil it around the center hub. The advantages of this folding pattern include that the fold lines are perpendicular to the radial forces, the web is deployed in a predictable sequential way and the coiling off takes advantage of the rotation instead of yielding problems with the Coriolis force. Therefore, this thesis is mainly based on deployment of a large quadratic space web folded in this way, Fig. 3.10.

In the simulations presented in this section, the following data were assumed: the side length S=100 m, the mass of the center hub $m_h=100$ kg, the radius of the center hub $r_h=6.3$ m, the mass of the web $m_w=122$ kg and the mass in each corner $m_c=1$ kg. The web mass was obtained by assuming that the cables were made of the Zylon fibres in [144] and that the mesh width of the web was 30 mm. For the FE model, the elastic modulus of the Zylon cables $E_{ca}=180$ GPa, the density of the cables $\rho_{ca}=1540$ kg/m³, the cross-sectional area of the cables $A_{ca}=2.5/0.030\cdot0.123$ mm² and the mesh width 2.5 meter, were also included.

42 4. RESULTS

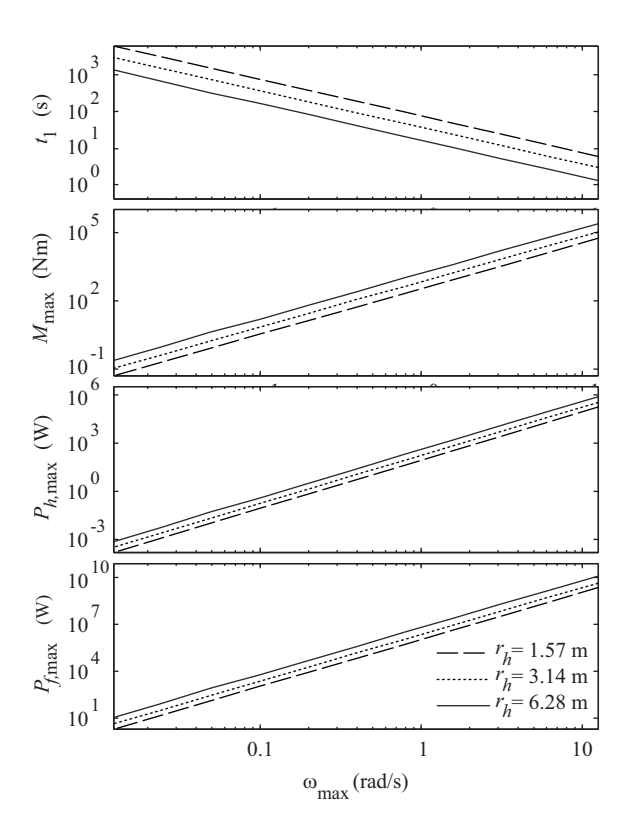


FIGURE 4.4. Torque and power requirements for arm deployment times.

Note that the cross-sectional area was adjusted so that the total mass of the web in the FE model was equal to that of a real web with 30 mm mesh width.

In paper 1, it was shown that the control strategy in Eq. (4.1) is promising also for the quadratic web, when the analytical model was used in the first phase of the deployment, i.e. the deployment of the arms. In paper 2, the feedback control was implemented in the objectiversion of LS-DYNA, and the FE model further demonstrated the applicability of this control law for the deployment of the arms. However, it was also shown that the second step requires tether control. On the other hand, if the whole web was deployed in one step, so that the web was always in tension, then the torque on the center hub was sufficient to obtain a controlled deployment, Fig. 4.2. In paper 2 it is also discussed how to apply the torque and explained how the analytical model can be used to determine the maximum torque and the power requirements for this control law, Fig. 4.4. As shown in paper 2, a major problem is that oscillations are induced if the torque is turned off before

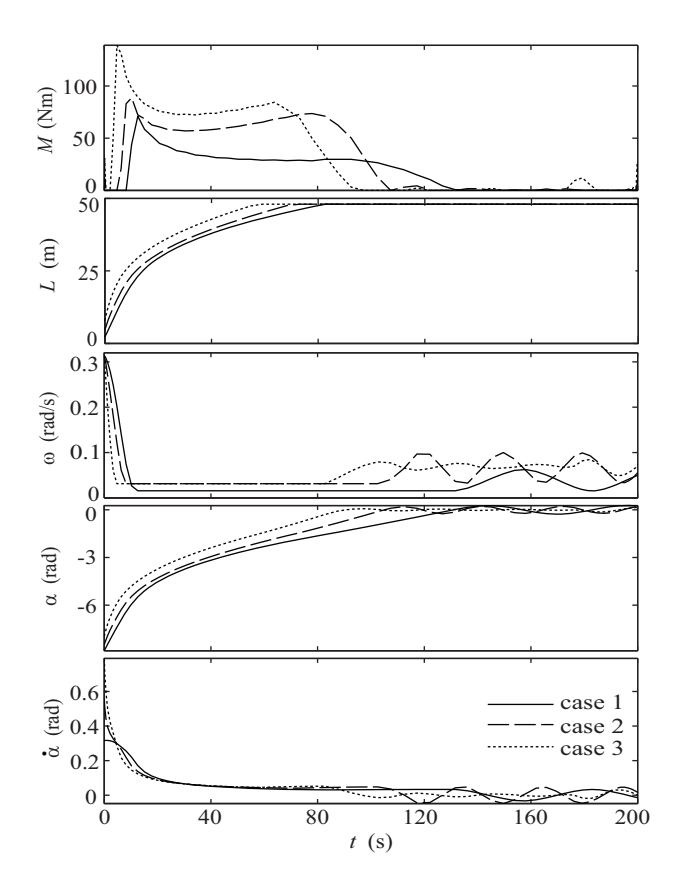


FIGURE 4.5. Different optimal controls for space web.

the arms, or strings of a continuous web, are in the radial direction, Fig. 4.3. The source of the oscillations were shown analytically in paper 2 for a case where $L \gg r$; if no damping is present, the hub-web system behaves like a harmonic oscillator.

Optimal control was therefore applied in paper 3 to find deployment trajectories that can reduce the oscillations, Fig. 4.5. The choice of objective function was extremely important for the results of the optimal control problems, and the final choice is a compromise between physical significance and computational convergence properties. For cases 1 and 2 in Fig. 4.5, the objective was to minimize the integral, for all t, of the squared torque. Also the constraints on the state and control variables had a significant impact on the results. The difference between cases 1 and 2 is that ω was allowed to fall to half the value in case 1 ($\omega_{\min} = \pi/20$) compared to case 2 ($\omega_{\min} = \pi/10$). Case 3 used the same constraints as case 2, but the objective was to minimize a combination between the integrals, for all t, of the squared torque and the squared difference $\omega - \omega_f$. All the three optimal control

44 4. RESULTS

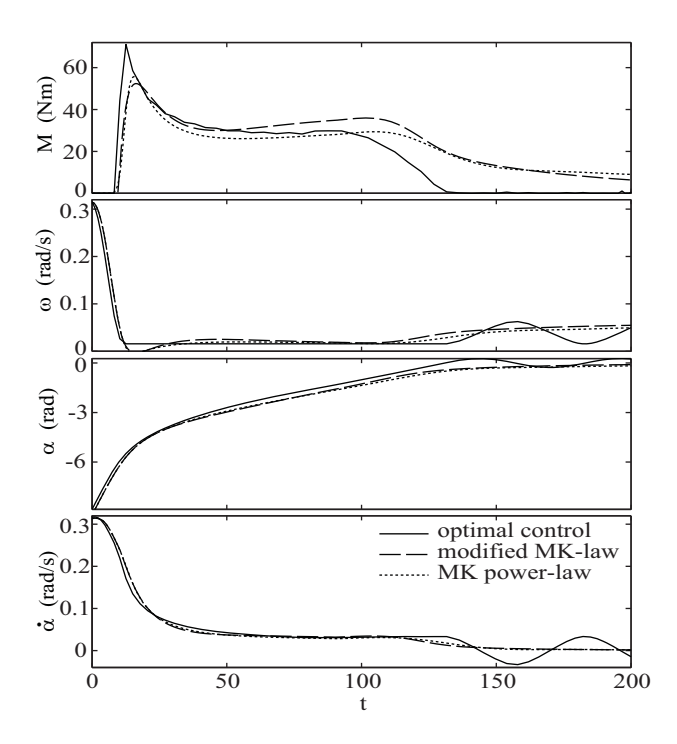


FIGURE 4.6. Optimal control law and control laws inspired by the optimal one.

curves suggest that no torque should be applied initially, then the torque should be increased rapidly to prevent the center hub from changing rotational direction. After reaching its maximum value, torque should be applied to keep the center hub rotating faster than the lowest acceptable level, $\omega = \omega_{\rm min}$. Finally, the torque should be turned off slowly when a sufficient amount of angular momentum has been supplied, so that the total angular momentum for the system is sufficiently high to keep the system rotating at the desired angular velocity.

Therefore, two new control laws were introduced in paper 3, the MK power-law

$$M = \widehat{M} \left(1 - \frac{\omega}{\omega_0} \right)^{\gamma} \tag{4.2}$$

and the modified MK-law

$$M = \max\left(0, \widehat{M}\left(1 - \frac{\omega}{\omega_f}\right)\right) \tag{4.3}$$

The agreement between the new control laws and the optimal control is shown in Fig. 4.6. In paper 3 it was also shown that the modified MK-laws are more robust

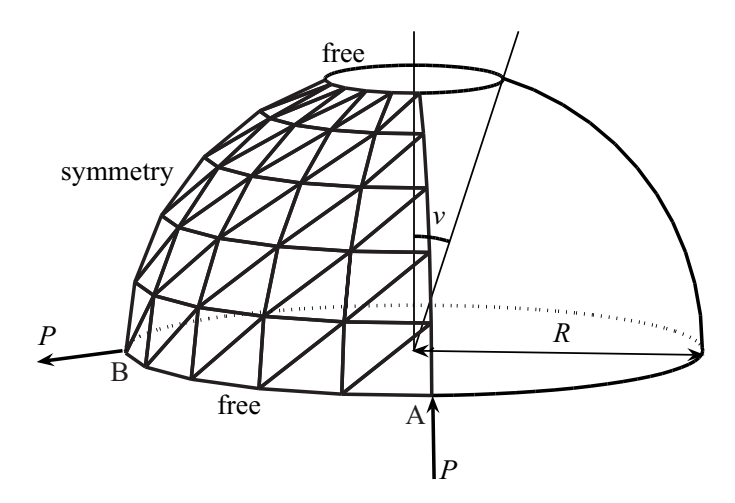


FIGURE 4.7. Hemispherical shell, mesh B. the bottom circumferential edge of the hemisphere is free. Because of symmetry only a quarter was modelled. Opposing radial point loads of P=2 N are applied, R=10 m, $v=\pi/10$, t=0.04 m, E=68.25 MPa and $\nu=0.3$.

than the original MK-law, because they decrease the risk of getting a changed rotational direction for the center hub. This could be verified with both the analytical model of the arm deployment and the FE model of the one-step deployment.

Control laws for combined torque and deployment rate control are also investigated in paper 3. A control law based on Hedgepeth's LOFT deployment [65] was derived. but its optimality was difficult to demonstrate.

Real-time control is briefly discussed in paper 3. For real-time control, it is not recommendable to follow a predetermined trajectory unless the dynamic model is very accurate. The dynamic model is rather accurate for arm deployment, but the deviation in the early stage of the deployment phase, where the control torque varies most rapidly, would make it costly in reality to follow the optimal angular velocity of the hub. Neither is it possible to use real-time optimal control because the convergence of the solution to the optimal control problem cannot be ensured.

4.2. Summary of the most important results from paper 4

The aim of the study in paper 4 was to find an RF shell element that is insensitive to element shape distortion. A thorough literature review was therefore performed. Because of their simplicity, the RF shell elements by Phaal and Calladine [130],

46 4. RESULTS

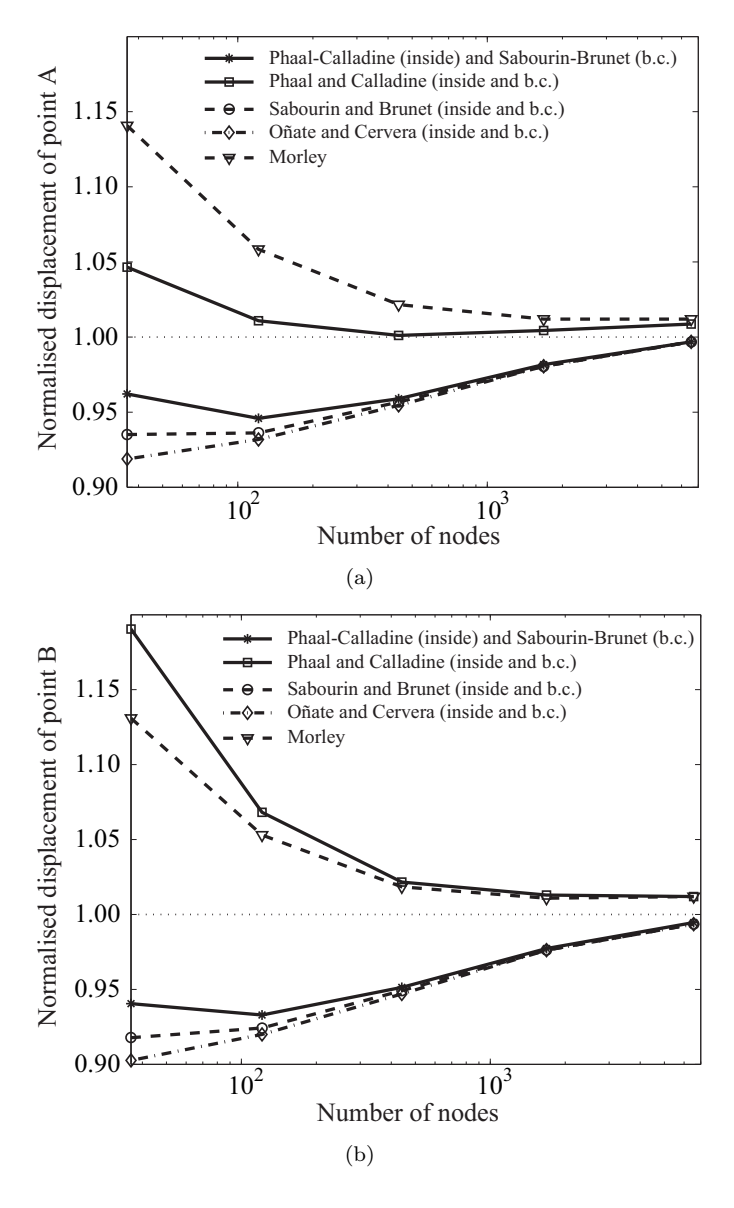


Figure 4.8. Hemispherical shell. The radial displacements at the loaded points are normalised with 0.0924 m.

Oñate and Cervera [123], Sabourin and Brunet [137], and Guo $et\ al.$ [59] were considered to be of certain interest to serve as a rapidly computed shell element with sufficient accuracy for thin films.

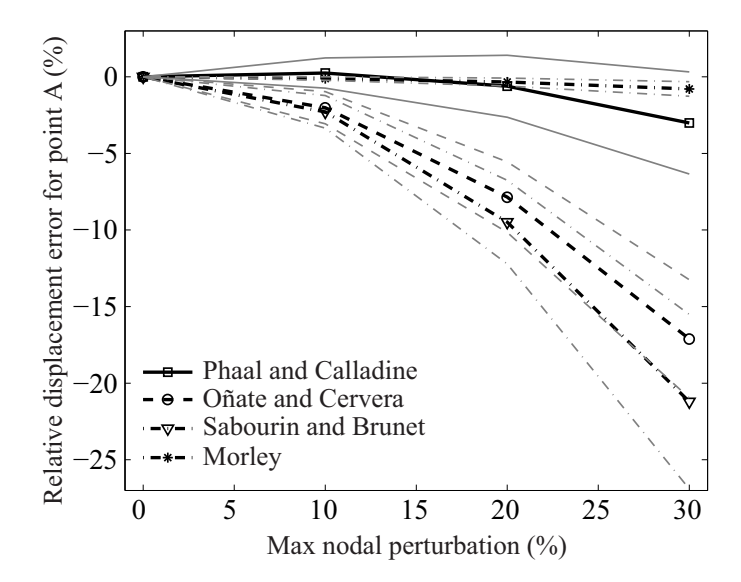


FIGURE 4.9. Hemispherical shell, unstructured mesh. Mean values (thick black lines) and 95% confidence intervals (thin grey lines) of the relative displacement error from 100 perturbed meshes.

We have earlier shown [46] that all the four mentioned RF shell element formulations yield the same stiffness matrix for uniform meshes if the same boundary conditions are used. However, differences are obtained for unstructured meshes since superposition of constant curvatures normal to each edge is an estimate of constant curvatures over the whole patch of elements. Only Phaal and Calladine [130] use the exact formulation, and it is not possible to obtain a more accurate curvature estimate for a plate bending element based on the six transversal DOF. Therefore, it is suggested that this element is used inside an unstructured mesh.

However, most publications about RF shell elements during the last decade have not considered the work by Phaal and Calladine as important. The reason for this is that the formulation by Phaal and Calladine did not show reliable convergence for all benchmark examples, and the solution was significantly more mesh-dependent than for the other RF elements. However, this is only due to their interpretation of the boundary conditions, which requires the use of fictitious nodes when one or two of the elements in a patch are missing. We have tried to improve the interpretation of the boundary formulations for this element, but the final proposal is to use an element that assumes constant curvatures normal to each edge as boundary element. For these elements, the boundary conditions (BC) follow naturally, see section 3.7 in paper 1. The element by Sabourin and Brunet is then preferred on the boundary since it is slightly more accurate than the element by Oñate and

48 4. RESULTS

Cervera for unstructured grids, and identical to that of Guo et al., but faster to compute.

The mesh of the Hemispherical shell, Figure 4.7, does not have elements of equal size. Therefore, differences between the four investigated elements are obtained even for the structured example, Figure 4.8. The elements by Morley and Phaal–Calladine, which reproduce constant curvatures exactly do also result in a too flexible solution due to the free edge BC. It can also be seen that the result for the element by Phaal and Calladine is more mesh-dependent than the others, which is due to the symmetry BC. The displacement when the elements on the boundary for Phaal and Calladine are changed to the element by Sabourin and Brunet is slightly better than the other RF elements. However, the differences become more evident when the nodes are perturbed from their original positions, Figure 4.9. The results from the other benchmark examples in [11] are presented in paper 4.

CHAPTER 5

Conclusions

5.1. Centrifugal force deployment

The many interesting applications that require new ingenious deployment and stiffening techniques for large lightweight structures in space motivate the research on centrifugal force deployment. The many unsuccessful experiments due to unexpected problems and the expense of performing realistic experiments motivate the requirement for new modelling techniques and simulation results. There is a need for both uncomplicated models, with few DOFs that can be used to understand and optimize the fundamental behavior of centrifugal force deployment, and more realistic models that can validate the results obtained with the simple models for realistic cases. The first problem that must be solved is to understand the dynamics, so that the membrane or web is controlled by the hub, and not the opposite. The second is to avoid entanglement, which is more difficult to model, but the risk can be decreased by an appropriate folding pattern and a minimum of oscillations during the deployment.

We have suggested dynamical models and optimal control laws for the centrifugal deployment of webs and membranes in space. The dynamical models assume webs or membranes that are either: (i) coiled around the hub and controlled by the angular velocity of the hub, or (ii) coiled onto spools and controlled by the angular velocity of the hub and the deployment rate. The first coiling method has the advantages that it includes less mechanisms that can fail or cause entanglement, the deployment rate can be higher because the Coriolis force does not cause entanglement, and it is easier to coil a large web or membrane around the hub than onto smaller spools. The second method has the advantage that it includes more redundancy because such control can be used to limit the deployment rate, which could be important if ω decreases very rapidly towards zero. The second method is also advantageous for coiling reasons if split membranes are used.

Tracking a predetermined trajectory is probably not recommended because trajectory tracking assumes that the dynamics is very accurately modeled. Therefore, control laws based on simple physical feedback relations are preferred over optimal control-based laws. For webs and membranes coiled on spools, a law similar to the one introduced by Hedgepeth [65] can be used to obtain non-transient deployment. If the web or membrane instead is coiled around the center hub, one proposed control law introduce a power of the ω -dependence of the MK-law. Another proposed law suggest that ω_0 is replaced with ω_f in the MK-law and M=0 for $\omega \geq \omega_f$. The results show that the control laws are almost identical to the optimal control law for certain parameter values, even though the simplicity of the MK-law remains.

The dynamical model can be used to determine the important \widehat{M} for the MK-laws and to simulate the deployment. Because of their simplicity, the MK-laws can be implemented in an FE software that allows feedback control or user-defined loads. The FE simulation results can then be used to increase \widehat{M} if required due to perturbations or model imperfections. For a real application, a safety margin is also required. However, a too high \widehat{M} also gives rise to oscillations.

The response time, from the measurement of the rotational velocity of the hub to the torque application, was neglected. Should a significant time lag exist, it implies that the steep gradient of the torque, proposed by the optimal control and the modified MK-laws for the early phase of the deployment, increases the risk of failure. Especially because the torque gradient coincides with the most critical phase of the deployment, i.e. when $\omega \to 0$. To minimize this risk, a slow deployment should be chosen.

The new control strategies were derived for simple examples. However, the new control laws based on the MK-law were useful also for the one-step deployment in the FE model, so it is expected to be applicable to many different folding patterns and deployment schemes.

5.2. Rotation-free elements

The element by Phaal and Calladine [130], with modified boundary elements, is proposed as an RF element for unstructured grids. The study in paper 1 showed that this element performs better than other RF elements for standard benchmark examples when unstructured meshes are used. We also showed the reason behind this, i.e. it approximates constant curvatures directly, instead of using superposition of constant curvatures normal to the edges. The former boundary conditions made the element by Phaal and Calladine dependent on the mesh orientation. Changing the elements along the boundary to another RF element improves the convergence and makes it less sensitive to the orientation of the mesh. We show the cause of this: (i) for free boundaries, the moment should not be zero for a patch, since all the three hinge angles contribute to the moments, and (ii) for symmetric boundaries, the stiffness is more evenly distributed between the nodes when superposition of the edge contributions is used compared to when fictitious nodes are used.

CHAPTER 6

Future research

6.1. Centrifugal force deployment

For centrifugal force deployment, there are many types of simulations that would be interesting to do and many model improvements that can be made. Some of them are:

- Three-dimensional modelling in the FE model, i.e. hub not restricted to 2D motion.
- Assymmetric initial geometries or asymmetric loading in the FE model.
- Include elasticity in the radial direction in the analytical model.
- Use a smaller hub compared to the web size. Now the smallest centre hub size is limited by the mesh size. In the future, the computations can be performed faster.
- Include contact between web members. It is extremely important to find a way to model the coiled space web near the center hub, and to simultaneously include contact in the initial state. Unfortunately, this is not trivial because improvement of one leads to problems with the other. One short-cut could be to model the web as a membrane.

6.2. Rotation-free elements

There are many possibilities to continue the review, refinement and development of RF elements, some of them are:

- Introduce the refined element by Phaal and Calladine in a commercial software, such as LS-DYNA. Routines exist in version 971 where a user-defined element can be introduced. However, it is not possible to include the essential information from the neighbouring elements. If it would be possible, the element could be used to simulate the deployment of complicated inflatable structures using the framework of the FE program.
- Extend the applicability of the refined element by Phaal and Calladine, to non-linear large displacements. This can be done using a co-rotational formulation.
- Eventually, develop an RF shell element that takes into account the coupling of bending and membrane effects as the element by Rio et al. [84], but use constant curvatures over the whole patch as Phaal and Calladines element. However, some of the simplicity with the element would then be lost.

Acknowledgment

First of all, I would like to thank my two supervisors, Dr. Gunnar Tibert and Professor Anders Eriksson, for sharing their knowledge and inspiring me to find new knowledge. Gunnar, I would like to thank you for your time and patience, for finding interesting research topics, making me believe in the importance of the work we do, for most of the literature studies behind the articles, for writing parts of the papers included in this thesis and for proof reading our articles and this thesis so many times. I would also like to thank you for being a friend but still being decisive in your leadership. My deepest gratitude also to you Anders for inspiration, support and giving me the opportunity to be a member of your research group. I could go on writing about my gratitude forever, but it can all be summarized in the facts that I wouldn't be here without you and if I would do this again I would choose you two as my supervisors!

All friends and colleagues at the Department of Mechanics also have a special place in my heart and mind. Thank you for all exciting and joyful lunches and coffee breaks. A special thanks to my former and present office mates Robert, Niklas, Carl-Ola, Olivier, Ori and Markus, you made it a pleasure to come to the office every day. A special thanks also to everybody in our research group for the friendly and creative atmosphere that you are contributing to.

To all friends that makes my life worth living: if you didn't know it before, you mean everything to me. Perhaps this is not the forum to thank all friends that I am training with, but without you I wouldn't have had the energy to write this thesis.

Finally, I would like to thank my family for support and belief in me when I grew up and when I need it the most. Thank you mum, dad, Martin and Tobias! There is nothing more I could have wanted from you, there is not much that I wouldn't like to share with you. I hope you share my happiness in this moment. Thank you!

Bibliography

- NASA NanoSail-D Home page, NanoSail-D/PRESat Update. http://www.nasa.gov/mission_pages/smallsats/nanosaild.html [retrived 3 Nov. 2008], 2008
- [2] ADOUM, M., AND LAPOUJADE, V. Examples' manual for *USER_LOADING option. In Proceedings of the 4th European LS-DYNA Users Conference (Ulm, Germany, May 2003).
- [3] ALEXANDER, D., SANDMAN, A., LIEWER, P., AYON, J., GOLDSTEIN, B., MURPHY, N., AND ET AL., M. V. Solar polar imager: Observing solar activity from a new perspective. In Proceedings of Solar Wind 11/SOHO 16 - Connecting Sun and Heliosphere (2005), no. 592 in ESA Special publication, pp. 663–666.
- [4] ALLMAN, D. A compatible triangular element including vertex rotations for plane elasticity analysis. Computers and Structures 19 (1984), 1–8.
- [5] ARITA, K., HASHIGUCHI, S., AND MIYAZAKI, Y. Evaluation of deployment method of spindeployable membrane. In Proc. 17th ISAS/JAXA Workshop on Astrodynamics and Flight Mechanics (Tokyo, 23–24 July 2007). Paper B-21.
- [6] BARKOW, B., STEIDL, A., TROGER, H., AND WIEDERMANN, G. Various methods of controlling the deployment of a tethered satellite. *Journal of Vibration and Control 9* (2003).
- [7] BARNES, M. R. Form-finding and analysis of tension space structures by dynamic relaxation. PhD thesis, Department of Civil Engineering, The City University, London, 1977.
- [8] BATOZ, J., BATHE, K., AND HO, L. A study of three-node triangular plate bending elements. International Journal for Numerical Methods in Engineering 15 (1980), 1771–1812.
- [9] BAZELEY, G., CHEUNG, Y., IRONS, B., AND ZIENKIEWICZ, O. Triangular elements in platebending-conforming and non-conforming solutions. In *Proceedings Conference on Matrix Methods in Structural Mechanics* (1966), pp. 547–576. AFFDL-TR-66-80.
- [10] BELYTSCHKO, T., STOLARSKI, H., AND CARPENTER, N. A C⁰ triangular plate element with one quadrature. International Journal for Numerical Methods in Engineering 20 (1984), 787–802.
- [11] BELYTSCHKO, T., STOLARSKI, H., LIU, W. K., CARPENTER, N., AND ONG, J. S. J. Stress projection for membrane and shear locking in shell finite elements. *Computer Methods in Applied Mechanics and Engineering* 51 (1985), 221–258.
- [12] Benson, D., Huntington, G., Thorvaldsen, T., and Rao, A. Direct trajectory optimization and costate estimation via an orthogonal collocation method. *Journal of Guidance*, Control and Dynamics 29, 6 (2006).
- [13] BERGAMIN, L., AND IZZO, D. Comments on deployment and control of charged space webs. ACT, ACT-TNT-MAD-CDCCSW07, Noordwijk, The Netherlands, Sep. 2007.
- [14] Betts, J. Survey of numerical methods for trajectory optimization. Journal of Guidance, Control and Dynamics 21, 2 (1998), 193–207.
- [15] BRUNET, M., AND SABOURIN, F. A simplified triangular shell element with a necking criterion for 3-D sheet-forming analysis. *Journal of Materials Processing Technology* 50 (1995), 238– 251.
- [16] BRUNET, M., AND SABOURIN, F. Analysis of a rotation-free 4-node shell element. International Journal for Numerical Methods in Engineering 66 (2006), 1483–1510.

- [17] BURTON, R. L., COVERSTONE, V. L., HARGENS-RYSANEK, J., ERTMER, K. M., BOTTER, T., BENAVIDES, G., WOO, B., CARROLL, D. L., GIEROW, P. A., FARMER, G., AND CARDIN, J. UltraSail ultra-lightweight solar sail concept. In *Proceedings of the 41st AIAA/ASME/SAE/ASEE Joint Propulsion Conference* (Tucson, AZ, July 2005), AIAA-2005-4117.
- [18] CASSAPAKIS, C. G., AND THOMAS, M. Inflatable structures technology overview. Tech. Rep. 95–3738, AIAA, 1995.
- [19] CHAN, A. S. L., AND DAVIES, G. A. O. A simplified finite element model for the impact of thin shells. In Structures under Shock and Impact, Proc. 1st Int. Conf. (Cambridge, MA, USA, 11–13 July 1989), P. S. Bulson, Ed., pp. 365–380.
- [20] CIRAK, F., AND ORTIZ, M. Fully C¹-conforming subdivision elements for finite deformation thin-shell analysis. *International Journal for Numerical Methods in Engineering* 51 (2001), 813–833.
- [21] CIRAK, F., ORTIZ, M., AND SCHRÖDER, P. Subdivision surfaces: a new paradigm for thin shell finite-element analysis. *International Journal for Numerical Methods in Engineering* 47 (2000), 2039–2072.
- [22] Comsol AB. Comsol optimization lab, version 1.1. Stockholm, Sweden, 2007.
- [23] Comsol AB. Comsol script 1.3.0.494. Stockholm, Sweden, 2008.
- [24] CONWAY, B. Discrete approximations to optimal trajectories using direct transcription and nonlinear programming. *Journal of Guidance, Control and Dynamics* 15, 4 (1992), 994– 1002.
- [25] COOK, R. D., MALKUS, D. S., PLESHA, M. E., AND WITT, R. J. Concepts and Applications of Finite Element Analysis, 4th ed. John Wiley & Sons, New York, 2002.
- [26] COTTER, T. An encomium on solar sailing. Report No. LA-5231-MS, Los Alamos National Laboratory, Los Alamos, NM, USA, May 1958. online: http://www.fas.org/sgp/othergov/doe/lanl/docs1/00390190.pdf [retrieved 7 Nov. 2008].
- [27] DACHWALD, B., OHNDORF, A., AND WIE, B. Solar sail trajectory optimization for the Solar Polar Imager (spi) mission. In *Proceedings of the AIAA/AAS Astrodynamics specialists* conference and exhibit (Keystone, CO, USA, Aug. 2006). AIAA 2006-6177.
- [28] DENAVIT, J., AND HARTENBERG, R. S. A kinematic notation for lower-pair mechanisms based on matrices. Journal of Applied Mechanics, Transactions of the ASME 22 (1955), 215–221.
- [29] Dontchev, A., Hager, W., and Veliov, V. Second order Runge-Kutta approximations in control constrained optimal control. SIAM Journal of Numerical Analysis 38, 1 (2000).
- [30] Dung, N., and Wells, G. Geometrically nonlinear formulation for thin shells without rotation degrees of freedom. Computer Methods in Applied Mechanical Engineering 197, 33–40 (2008).
- [31] ELDER, D. C. Out from behind the eight-ball: a history of Project Echo, vol. 16 of American Astronautical Society History Series. Univelt, San Diego, CA, USA, 1995.
- [32] ELNAGAR, J., KAZEMI, M. A., AND RAZZAGHI, M. The pseudospectral Legendre method for discretizing optimal control problems. *IEEE Transactions on Automatic Control* 40, 10 (1995), 1793–1796.
- [33] FAHROO, F., AND ROSS, I. Pseudospectral methods for infinite horizon nonlinear optimal control problems. In 2005 AIAA Guidance, Navigation and Control Conference (San Francisco, CA, Aug. 2005), AIAA Paper 2005-6076.
- [34] FAHROO, F., AND ROSS, I. M. Costate estimation by a Legendre pseudospectral method. Journal of Guidance, Control and Dynamics 24, 2 (2001), 270–277.
- [35] FAHROO, F., AND ROSS, I. M. Direct trajectory optimization by a chebyshev pseudospectral method. Journal of Guidance, Control and Dynamics 25, 1 (2002), 160–166.
- [36] FLORES, F., AND ESTRADA, C. A rotation-free thin shell quadrilateral. Computer Methods in Applied Mechanical Engineering 196, 25-28 (2007).

- [37] FLORES, F. G., AND OÑATE, E. Improvements in the membrane behaviour of the three node rotation-free BST shell triangle using an assumed strain approach. Computer Methods in Applied Mechanics and Engineering 194 (2005), 907–932.
- [38] FLORES, F. G., AND OÑATE, E. Rotation-free element for the non-linear analysis of beams and axisymmetric shells. Computer Methods in Applied Mechanics and Engineering 195 (2006), 5297–5315.
- [39] FORWARD, R. Roundtrip interstellar travel using laser-pushed lightsails. Journal of Spacecraft and Rockets 21, 2 (1984).
- [40] FREELAND, R. Gossamer Spacecraft: Membrane and Inflatable Structures Technology for Space Applications, vol. 191 of Progress in Astronautics and Aeronautics. AIAA, Reston, VA, USA, 2001, ch. 2, pp. 35–47.
- [41] FREELAND, R. E., AND VEAL, G. R. Significance of the inflatable antenna experiment technology. In Proc. 39th AIAA/ASME/ASCE/AHS/ASC Structures, Structural Dynamics, and Materials Conf. (Long Beach, CA, USA, April 20–23 1998). AIAA-98-2104.
- [42] FRIEDMAN, L., CARROLL, W., GOLDSTEIN, R., JACOBSON, R., KIEVIT, J., LANDEL, R., LAYMAN, W., MARSH, E., PLOSZAJ, R., ROWE, W., RUFF, W., STEVENS, J., STIMPSON, L., TRUBERT, M., VARSI, G., AND et al., J. W. Solar sailing - the concept made realistic. AIAA paper 78–82, Jan. 1978.
- [43] FUJII, H. A., AND ANAZAWA, S. Deployment/retrieval control of tethered subsatellite through an optimal path. *Journal of Guidance, Control and Dynamics* 17, 6 (1994).
- [44] FURUYA, H., AND INOUE, Y. Tether controlled deployment characteristics of rotationally skew fold membrane for spinning solar sail. In Proc. 15th IASA/JAXA Workshop on Astrodynamics and Flight Mechanics (Tokyo, 25–26 July 2005). Paper B-1.
- [45] GÄRDSBACK, M. Rotation-Free Shell Elements for Thin-Film Structures and Simulations of Centrifugally Deployed Space Webs. Licentiate thesis, ISRN KTH/MEK/TR-07/02-SE, Royal Institute of Technology, Stockholm, Sweden, 2007.
- [46] GÄRDSBACK, M., AND TIBERT, G. Evaluation of triangular shell elements for thin membrane structures. In *Proc. 5th International Conference on Computation of Shell & Spatial Structures* (Salzburg, Austria, 1–4 June, 2005).
- [47] GÄRDSBACK, M., AND TIBERT, G. A comparison of rotation-free triangular shell elements for unstructured meshes. Computer Methods in Applied Mechanical Engineering 196, 49–52 (2007), 5001–5015.
- [48] GÄRDSBACK, M., AND TIBERT, G. Deployment control of spinning space webs. *Journal of Guidance, Control and Dynamics* (2008). accepted for publication.
- [49] GÄRDSBACK, M., TIBERT, G., AND IZZO, D. Design considerations and deployment simulations of spinning space webs. In Proceedings of the 48th AIAA/ASME/ASCE/AHS/ASC Structures, Structural Dynamics, and Materials Conference (Honolulu, HW, Vol. 2, Apr. 2007), AIAA-2007-1829, pp. 1503-1512.
- [50] GARWIN, R. Solar sailing: A practical method of propulsion within the solar system. Jet Propulsion 28 (1958).
- [51] GILL, P., MURRAY, W., AND SAUNDERS, M. SNOPT: An SQP algorithm for large-scale constrained optimization. SIAM Journal on Optimization 12, 4 (1997), 979–1006.
- [52] GILL, P., MURRAY, W., AND SAUNDERS, M. User's guide for SNOPT version 7: Software for large-scale nonlinear programming. Tech. rep., 2006.
- [53] GILL, P., MURRAY, W., AND SAUNDERS, M. User's guide for SQOPT version 7: Software for large-scale linear and quadratic programming. Tech. rep., 2006.
- [54] GLASER, P. Power from the sun: its future. Science 162, 3856 (1968).
- [55] GLASER, P. Method and appatus for converting solar radiation to electrical power, Dec. 25 1973. United States Patent 3,781,647.
- [56] Gong, Q., Kang, W., and Ross, I. M. A pseudospectral method for the optimal control of constrained feedback linearizable systems. *IEEE Transactions on Automatic Control* 51, 7 (2006), 1115–1129.

- [57] GONG, Q., ROSS, I. M., KANG, W., AND FAHROO, F. Connections between the covector mapping theorem and convergence of pseudospectral methods for optimal control. Computational Optimization and Applications (2008). doi: 10.1007/s10589-007-9102-4, online first.
- [58] GROSSMAN, J. Solar sailing: the next space craze? Engineering & Science, 4 (2000), 18-29.
- [59] Guo, Y. Q., Gati, W., Naceur, H., and Batoz, J. L. An efficient DKT rotation free shell element for springback simulation in sheet metal forming. *Computers and Structures* 80 (2002), 2299–2312.
- [60] HALLQUIST, J. O. LS-DYNA theory manual. Livermore Software Technology Corporation.
- [61] HAMPSHIRE, J. K., TOPPING, B. H. V., AND CHAN, H. C. Three node triangular bending elements with one degree of freedom per node. *Engineering Computations 9* (1992), 49–62.
- [62] HARGRAVES, C., AND PARIS, S. Direct trajectory optimization using nonlinear programming and collocation. *Journal of Guidance, Control and Dynamics* 10, 4 (1987).
- [63] HAUPTMANN, R., AND SCHWEIZERHOF, K. A systematic development of solid-shell element formulations for linear and non-linear analysis employing only displacement degrees of freedom. *International Journal for Numerical Methods in Engineering* 42 (1998), 49–69.
- [64] HEATON, A. Solar sail roadmap mission GN&C challenges. In Proceedings of the AIAA guidance, navigation and control conference and exhibit (San Francisco, CA, USA, Aug. 2005). AIAA 2005-6170.
- [65] HEDGEPETH, J. M. Dynamics of a large spin-stiffened deployable paraboloidal antenna. Journal of Spacecraft and Rockets 7, 9 (1970), 1043–1048. doi: 10.2514/3.30100.
- [66] HEDGEPETH, J. M., MACNEAL, R. H., AND SCHUERCH, H. U. Heliogyro solar sailer summary report. NASA CR-1329, June 1969.
- [67] HERENDEEN, R., KARY, T., AND REBITZER, J. Energy analysis of the solar power satellite. Science 205, 4405 (1979).
- [68] HUGHES, T., TAYLOR, R., SACKMAN, J., CURNIER, A., AND KANOKNUKULCHAI, W. A finite element method for a class of contact-impact problems. Computer Methods in Applied Mechanical Engineering 8, 3 (1976), 249–276. doi: 10.1016/0045-7825(76)90018-9.
- [69] INAGAWA, S., AND MATUNAGA, S. On-ground dynamics simulator for spinning solar sail. In Proc. 18th IASA/JAXA Workshop on Astrodynamics and Flight Mechanics (Tokyo, 28–29 July 2008). Paper A-7.
- [70] INMAN, D., AND RUGGIERO, E. Gossamer spacecraft: Recent trends in design, analysis, experimentation, and control. *Journal of Spacecraft and Rockets* 43, 1 (2006).
- [71] Institute for Handling Devices and Robotics, Vienna University of Technology. SPS (solar power satellite)—Roby space, September 4 2006. Online Internet: http://www.ihrt.tuwien.ac.at/robyspace/.
- [72] JENKINS, C. H. M., Ed. Gossamer spacecraft: membrane and inflatable structures technology for space applications, vol. 191 of Progress in Astronautics and Aeronautics. AIAA, Reston, VA. USA, 2001.
- [73] JENKINS, C. H. M., Ed. Recent Advances in Gossamer Spacecraft, vol. 212 of Progress in Astronautics and Aeronautics. AIAA, Reston, VA, USA, 2006.
- [74] JOHNSON, L., YOUNG, R., AND IV, E. M. Recent advances in solar sail propulsion systems at nasa. Acta Astronautica 61 (2007).
- [75] JONES, T. C., BART-SMITH, H., MIKULAS, M., AND WATSON, J. Finite element modeling and analysis of large pretensioned space structures. *Journal of Spacecraft and Rockets* 44, 1 (2007), 183–193. doi: 10.2514/1.23116.
- [76] KANEMITSU, T., MATSUMOTO, S., NAMBA, H., SATO, T., TADOKORO, H., OURA, T., TAKAGI, K., AOKI, S., AND KAYA, N. Self-deployable antenna using centrifugal force. In *IUTAM-IASS Symp. on Deployable Structures: Theory and Applications* (Cambridge, UK, 6–9 September 1998), S. Pellegrino and S. D. Guest, Eds., Kluwer Academic Publishers, Dordrecht, The Netherlands, 2000, pp. 173–182.

- [77] KANG, W., ROSS, I. M., AND GONG, Q. Pseudospectral Optimal Control and Its Convergence Theorems. Springer Berlin Heidelberg, Heidelberg, Germany, 2008, ch. 2.4, pp. 109–124. doi: 10.1007/978-3-540-74358-3-8.
- [78] KAYA, N., IWASHITA, M., NAKASUKA, S., SUMMERER, L., AND MANKINS, J. Crawling robots on large web in rocket experiment on Furoshiki deployment. In *Proceedings of the 55th In*ternational Astronautical Congress (Vancouver, Canada, Vol. 10, Oct. 2004), International Astronautical Federation, IAC-04-R3, pp. 663-667.
- [79] KISHIMOTO, N., NATORI, M. C., HIGUCHI, K., AND UKEGAWA, K. New deployable membrane structure models inspired by morphological changes in nature. In *Proceedings of the 47th AIAA/ASME/ASCE/AHS/ASC Structures, Structural Dynamics, and Materials Conference* (Newport, RI, Vol. 5, May 2006), AIAA-2006-1898, pp. 3722-3725.
- [80] Knight, Jr., N. F. Raasch challenge for shell elements. AIAA Journal 2 (1997), 375–381.
- [81] KYSER, A. C. Uniform-stress spinning filamentary disk. AIAA Journal 3, 7 (1965), 1313–1316. doi: 10.2514/3.3129; also NASA CR-106, July 1964.
- [82] Landis, G. Interstellar flight by particle beam. Acta Astronautica 55 (2004).
- [83] LANG, W. E., AND HONEYCUTT, G. H. Simulation of deployment dynamics of spinning spacecraft. NASA TN-D-4074, Aug. 1967.
- [84] LAURENT, H., AND RIO, G. Formulation of a thin shell finite element with continuity C⁰ and convected frame notion. Computational Mechanics 27 (2001), 218–232.
- [85] LIVERMORE SOFTWARE TECHNOLOGY CORPORATION. LS-DYNA v971.7600.1224, double precision. Livermore, CA, 2007.
- [86] MACNEAL, R., AND HARDER, R. A proposed standard set of problems to test finite element accuracy. Finite Elements in Analysis and Design 1 (1985), 3–20.
- [87] MACNEAL, R. H. The Heliogyro: an interplanetary flying machine. NASA CR-84460, March 1967.
- [88] MACNEAL, R. H. Structural dynamics of the Heliogyro. NASA CR-1745, May 1971.
- [89] Mankins, J. Space-based solar power: architectural and system considerations. In Proceedings of the 6th International Energy Conversion Engineering Conference (Cleveland, Ohio, July 2008). AIAA 2008-5600.
- [90] Mankins, J. C. A fresh look at space solar power: New architectures, concepts and technologies. Acta Astronautica 41, 4–10 (1997). doi:10.1016/S0094-5765(98)00075-7.
- [91] Mankins, J. C. A technical overview of the "suntower" solar power satellite concept. Acta Astronautica 50, 6 (2002). doi:10.1016/S0094-5765(01)00167-9.
- [92] Maplesoft, Waterloo Maple, Inc. Maple 11.01. Waterloo, Canada, 2007.
- [93] MASUMOTO, S., OMAGARI, K., YAMANAKA, T., AND MATUNAGA, S. System configuration of tethered spinning solar sail for orbital experiment: numerical simulation and ground experiment. In *Proceedings of the 25th International Symposium on Space Technology and Science (ISTS)* (Kanazawa City, Japan, June 2006).
- [94] MATLOFF, G., VULPETTI, G., BANGS, C., AND HAGGERTY, R. The interstellar probe (isp): Pre-perihelion trajectories and application of holography. NASA/CR-2002-211730, June 2002.
- [95] Matsumoto, H. Research on solar power satellites and microwave power transmission in japan. IEEE Microwave Magazine 3, 4 (2002). doi: 10.1109/MMW.2002.1145674.
- [96] MATUNAGA, S., MORI, O., NAKAYA, K., IAI, M., OMAGARI, K., AND YABE, H. New spinning deployment method of large thin membranes with tether control. In *Proceedings of the* 54th International Astronautical Congress (Bremen, Germany, Vol. 1, Sep.—Oct. 2003), International Astronautical Federation, IAC-03-A.4.01, pp. 257–260.
- [97] MATUNAGA, S., YABE, H., NAKAYA, K., IAI, M., OMAGARI, K., AND MORI, O. Membrane deployment for spinning formation-flight solar sail. In *Proceedings of the 14th Workshop on Astrodynamics and Flight Mechanics* (Tokyo, July 2004).

- [98] McDonald, M., Hughes, G., McInnes, C., Lyngvi, A., Falkner, P., and Atzei, A. Solar polar orbiter: a solar sail technology reference study. *Journal of Spacecraft and Rockets* 43, 5 (2006).
- [99] McInnes, C. Solar sailing: technology, dynamics and mission applications. Praxis Publishing, Chichester, UK, 1999.
- [100] MCKENZIE, D., AND CARTMELL, M. Modelling of tethered space-web structures. Journal of the British Interplanetary Society 61 (2008), 24–31.
- [101] MCKENZIE, D., CARTMELL, M., RADICE, G., AND VASILE, M. Space Webs: Final Report. ESA/ACT, Adriana ID: 05/4109b, Noordwijk, The Netherlands, 2006.
- [102] McSpadden, J. Summary of recent results from NASA's space solar power (SPS) programs and the current capabilities of microwave WPT technology. Tech. rep., 2002.
- [103] MELNIKOV, V. M., AND KOSHELEV, V. A. Large space structures formed by centrifugal forces, 1 ed., vol. 4 of Earth Space Institute Book Series. Gordon and Breach Science Publishers, Amsterdam, The Netherlands, 1998, pp. 21–61.
- [104] MITSUGI, J., NATORI, M., AND MIURA, K. Preliminary evaluation of the spinning solar sail. In Proceedings of the 28th AIAA/ASME/ASCE/AHS/ASC Structures, Structural Dynamics, and Materials Conference (Monterey, CA, April 1987), AIAA-1987-742.
- [105] MIYAZAKI, Y. Dynamic behavior of spinning solar sail. In Proc. 18th IASA/JAXA Workshop on Astrodynamics and Flight Mechanics (Tokyo, 28–29 July 2008). Paper A-7.
- [106] MIYAZAKI, Y., AND IWAI, Y. Dynamics model of solar sail membrane. In Proceedings of the 14th Workshop on Astrodynamics and Flight Mechanics (Tokyo, July 2004).
- [107] MORI, O., NAKANOH, T., TARAO, K., SHIDA, M., TSUDA, Y., SAIKI, T., AND KAWAGUCHI, J. Static deployment experiment of large membrane for solar sail spacecraft. In Proc. 15th IASA/JAXA Workshop on Astrodynamics and Flight Mechanics (Tokyo, 25–26 July 2005). Paper B-2.
- [108] MORI, O., NISHIMAKI, S., MATSUMOTO, M., IWAKURA, A., ARAKAWA, M., OKADA, S., SHIBASAKI, Y., SHIRASAWA, Y., HANAOKA, F., AND SUGITA, M. Asymmetric deployment dynamics of large membrane. In Proc. 16th IASA/JAXA Workshop on Astrodynamics and Flight Mechanics (Tokyo, 1–2 August 2006). Paper C-17.
- [109] MORI, O., SAWADA, H., TSUDA, Y., FUNASE, R., KAWAGUCHI, J., F.HANAOKA, MATSUMOTO, M., OKADA, S., SHIBASAKI, Y., SHIRASAWA, Y., KITAJIMA, A., HIRABAYASHI, M., MIWA, Y., TRIWANT, S., ARAKAWA, M., AND SUGITA, M. Deployment demonstration of supersized membrane for spinning solar sail. In Proc. 17th ISAS/JAXA Workshop on Astrodynamics and Flight Mechanics (Tokyo, 23–24 July 2007). Paper B-20.
- [110] MORI, O., TSUDA, Y., NISHIMURA, Y., AND KAWAGUCHI, J. Deployment dynamics of clover type solar sail. In *Proceedings of the 14th Workshop on Astrodynamics and Flight Mechanics* (Tokyo, July 2004).
- [111] MORLEY, L. S. D. The constant-moment plate-bending element. Journal of Strain Analysis 6 (1971), 20–24.
- [112] Moses, H. Impacts of satellite power system technology. Energy 4, 5 (1979).
- [113] NAKANO, T., MORI, O., AND KAWAGUCHI, J. Stability of spinning solar sail-craft containing a huge membranes. In *Proceedings of the AIAA Guidance, Navigation, and Control Conference* (San Francisco, CA, Vol. 5, Aug. 2005), AIAA-2005-6182, pp. 3425-3437.
- [114] NAKASHNIO, K., AND NATORI, M. C. Shape characteristics of spin-stabilised structures under microgravity environment. In Proc. 42nd AIAA/ASME/ASCE/AHS/ASC Structures, Structural Dynamics, and Materials Conf. (Seattle, WA, USA, 16–19 April 2001). AIAA-2001-1344.
- [115] NAKASUKA, S., AOKI, T., IKEDA, I., TSUDA, Y., AND KAWAKATSU, Y. "Furoshiki Satellite" a large membrane structure as a novel space system. Acta Astronautica 48, 5–12 (2001), 461–468. doi: 10.1016/S0094-5765(01)00056-X.

- [116] NAKASUKA, S., FUNANE, T., NAKAMURA, Y., NOJIRA, Y., SAHARA, H., SASAKI, F., AND KAYA, N. Sounding rocket flight experiment for demonstrating "Furoshiki Satellite" for large phased array antenna. Acta Astronautica 59, 1–5 (2006), 200–205. doi: 10.1016/j.actaastro.2006.02.014.
- [117] NAKASUKA, S., FUNASE, R., NAKADA, K., KAYA, N., AND MANKINS, J. C. Large membrane "Furoshiki Satellite" applied to phased array antenna and its sounding rocket experiment. Acta Astronautica 58, 8 (2006), 395–400. doi: 10.1016/j.actaastro.2005.12.010.
- [118] Nakasuka, S., and Kaya, N. Quick release on experiment results of mesh deployment and phased array antenna by S-310-36. The Forefront of Space Science [online], Institute of Space and Astronautical Science, 2006. http://www.isas.ac.jp/e/forefront/2006/nakasuka/ [retrieved 4 Sep. 2006].
- [119] NAKAYA, K., MORI, O., TSUDA, Y., SAIKI, T., YAMAMOTO, T., AND KAWAGUCHI, J. Dynamic deployment of solar sail membrane with stiffness. In Proc. 15th IASA/JAXA Workshop on Astrodynamics and Flight Mechanics (Tokyo, 25–26 July 2005). Paper B-12.
- [120] Oda, M. Building a space solar power system. In Proceedings of 2nd International Conference on Recent Advances in Space Technologies (June 2005), pp. 24–27. doi:10.1109/RAST.2005.1512528.
- [121] OKUIZUMI, N., SAKAMOTO, K., KITAJIMA, A., AND SUGITA, M. Centrifugal deployment experiments of a square-shaped solar sail membrane. In Proc. 18th IASA/JAXA Workshop on Astrodynamics and Flight Mechanics (Tokyo, 28–29 July 2008). Paper A-5.
- [122] OÑATE, E., CENDOYA, P., AND MIQUEL, J. Nonlinear explicit dynamic analysis of shells using the BST rotation-free triangle. Engineering Computations 9(6) (2002), 662–706.
- [123] OÑATE, E., AND CERVERA, M. Derivation of thin plate bending elements with one degree of freedom per node: A simple three node triangle. *Engineering Computations* 10 (1993), 543–561.
- [124] OÑATE, E., AND FLORES, F. G. Advances in the formulation of the rotation-free basic shell triangle. Computer Methods in Applied Mechanics and Engineering 194 (2005), 2406–2443.
- [125] OÑATE, E., AND ZÁRATE, F. Rotation-free triangular plate and shell elements. International Journal for Numerical Methods in Engineering 47 (2000), 557–603.
- [126] ONODA, J., TAKEUCHI, S., AND AOKI, Y. A preliminary investigation of a spin-stabilised solar sail. In Proc. 45th AIAA/ASME/ASCE/AHS/ASC Structures, Structural Dynamics, and Materials Conf. (Palm Springs, CA, USA, April 19–22 2004). AIAA 2004-1511.
- [127] PALMERINI, G. B., SGUBINI, S., AND SABATINI, M. Space webs based on rotating tethered formations. In *Proceedings of the 57th International Astronautical Congress* (Valencia, Spain, Vol. 10, Oct. 2006), International Astronautical Federation, IAC-06-D1.1.04, pp. 6819-6828.
- [128] Peng, X., and Chrisfield, M. A consistent co-rotation formulation for shells using the constant stress/constant moment triangle. *International Journal for Numerical Methods in Engineering 35* (1992), 1829–1847.
- [129] Phaal, R., and Calladine, C. R. A simple class of finite elements for plate and shell problems. I: Elements for beams and thin flat plates. *International Journal for Numerical Methods in Engineering* 35 (1992), 955–977.
- [130] Phaal, R., and Calladine, C. R. A simple class of finite elements for plate and shell problems. II: An element for thin shells, with only translational degrees of freedom. *International Journal for Numerical Methods in Engineering 35* (1992), 979–996.
- [131] PONTRYAGIN, L., BOLTYANSKII, V., GAMKRELIDZE, R., AND MISCHENKO, E. The Mathematical Theory of Optimal Processes. Wiley-Interscience, New York, NY, 1962.
- [132] RAZZAQUE, A. Program for triangular bending elements with derivative smoothing. International Journal for Numerical Methods in Engineering 6 (1973), 333–343.
- [133] ROBBINS, JR., W. M. The feasibility of an orbiting 1500-meter radio telescope. NASA CR-792, June 1967.

- [134] ROELANDT, J. M., AND BATOZ, J. L. Shell finite element for deep drawing problems: computational aspects and results. In *IUTAM symposium on finite inelastic deformations* (1992), pp. 423–430.
- [135] Ross, I. M., And Fahroo, F. Legendre pseudospectral approximations of optimal control problems. Lecture Notes in Control and Information Sciences 295 (2004), 327–342.
- [136] RUSSELL, C. Deployment simulation of inflatable tensegrity frameworks. Master of Science Thesis, KTH Engineering Sciences, Royal Institute of Technology, Stockholm, Sweden, 2005.
- [137] SABOURIN, F., AND BRUNET, M. Analysis of plates and shells with a simplified three node triangular element. Thin-Walled Structures 21 (1995), 209–223.
- [138] Saito, Y., Fujita, T., and Mori, M. Summary of studies on space solar power systems of japan aerospace exploration agency (jaxa). In *Proceedings of the 57th International As*tronautical Congress (Valencia, Spain, Oct. 2006), International Astronautical Federation. IAC-06-C3.1.04.
- [139] SALAMA, M., KUO, C. P., AND LOU, M. Simulation of deployment dynamics of inflatable structures. AIAA Journal 38, 12 (2000), 2277–2283.
- [140] SALAMA, M., WHITE, C., AND LELAND, R. Ground demonstration of a spinning solar sail deployment concept. *Journal of Spacecraft and Rockets* 40, 1 (2003), 9–14.
- [141] SCHUERCH, H. U., AND HEDGEPETH, J. M. Large low-frequency orbiting radio telescope. NASA CR-1201, Oct. 1968.
- [142] SCHUERCH, H. U., AND MACNEAL, R. Deployable centrifugally stabilized structures for atmospheric entry from space. NASA CR-69, July 1964.
- [143] SCHWENK, F. Summary assessment of the satellite power system. Journal of Energy 7, 3 (1983).
- [144] SEELY, L. G., ZIMMERMAN, M., AND MCLAUGHLIN, J. The use of Zylon fibers in ULDB tendons. Advances in Space Research 33, 10 (2004), 1736–1740. doi: 10.1016/j.asr.2003.07.046.
- [145] Shirley, D. The mariner 10 mission to venus and mercury. Acta Astronautica 53, 4–10 (2003).
- [146] Shpakovsky, N. Space mirror. The TRIZ Journal [online] 7, 6 (2002). http://www.triz-journal.com/archives/2002/06/e/index.htm [retrieved 20 Feb. 2008].
- [147] SOUZA, D. M. Space sailing. Lerner Publications, Minneapolis, USA, 1993.
- [148] Summerer, L., Ayre, M., Galvez, A., Ongaro, F., and Vasile, M. Roles of solar power from space for Europe - space exploration and combinations with terrestrial solar plants concepts. In Proceedings of the 55th International Astronautical Congress of the International Astronautical Federation, the International Academy of Astronautics, and the International Institute of Space Law (Vancouver, British Columbia, Canada, Oct. 2004). IAC-04-R.1.03.
- [149] The Mathworks, Inc. Matlab 7.5.0.338 (r2007b). Natick, MA, 2007.
- [150] TIBERT, G., AND GÄRDSBACK, M. Space Webs: Final Report. ESA/ACT, Adriana ID: 05/4109a, Noordwijk, The Netherlands, 2006.
- [151] Trefethen, L. Spectral Methods in MATLAB. 1st ed., SIAM, Philadelphia, PA, 2000.
- [152] TSUDA, Y. Dynamics analysis of spinning solar sail. In Proc. 16th IASA/JAXA Workshop on Astrodynamics and Flight Mechanics (Tokyo, 1–2 August 2006). Paper C-18.
- [153] TSUDA, Y., AND MORI, O. Dynamics analysis of solar sail membrane using improved particle method. In Proc. 15th IASA/JAXA Workshop on Astrodynamics and Flight Mechanics (Tokyo, 25–26 July 2005). Paper B-3.
- [154] TSUDA, Y., NAKAYA, K., MORI, O., AND YAMAMOTO, T. Microsatellite-class solar sail demonstrator — mission design and development status. In *Proceedings of the 25th International Symposium on Space Technology and Science (ISTS)* (Kanazawa City, Japan, June 2006).
- [155] TURNER, M. J., CLOUGH, R. W., MARTIN, H. C., AND TOPP, L. J. Stiffness and deflection analysis of complex structures. J. Aeronautical Sciences 23(9) (1956), 805–823.
- [156] VIRDEE, L., JANSSON, G., KIS, R., GOODWIN, P., AND TEMPORELLI, P. Intelsat's next generation satellite for the americas. Acta Astronautica 48, 5–12 (2001).

- [157] VLASSENBROECK, J., AND DOOREN, R. V. A Chebyshev technique for solving nonlinear optimal control problems. IEEE Transactions on Automatic Control 33, 4 (1988).
- [158] WALLACE, R. A., AYON, J. A., AND SPRAGUE, G. A. Interstellar probe mission/system concept. In *IEEE Aerospace Conference Proceedings* (Big Sky, MT, Vol. 7, March 2000), IEEE, pp. 385–396.
- [159] WILLIAMS, P. Jacobi pseudospectral method for solving optimal control problems. *Journal of Guidance, Control and Dynamics* 27, 2 (2004), 293–297.
- [160] WILLIAMS, P. Optimal deployment/retrieval of a tethered formation spinning in the orbital plane. *Journal of Spacecraft and Rockets* 43, 3 (2006), 638–650.
- [161] WILLIAMS, P. Optimal deployment/retrieval of tethered satellites. Journal of Spacecraft and Rockets 45, 2 (2008), 324–343.
- [162] WRIGHT, J. L. Space sailing. Gordon and Breach Science Publications, Philadelphia, USA, 1992.
- [163] YANG, H., SAIGAL, S., MASUD, A., AND KAPANIA, R. A survey of recent shell finite elements. International Journal for Numerical Methods in Engineering 47 (2000), 101–127.
- [164] YOUNG, R. Updated Heliostorm warning mission: enhancements based on new technology. In Proceedings of the 48th AIAA/ASME/ASCE/AHS/ASC Structures, structural dynamics and materials conference (Honolulu, HI, USA, Apr. 2007). AIAA 2007-2249.

List of papers

This thesis contains the following papers:

Paper 1. GÄRDSBACK, M., TIBERT, G. AND IZZO, D., 2007

Design considerations and deployment simulations of spinning space webs.

Proceedings of the 48th AIAA/ASME/ASCE/AHS/ASC Structures, Structural Dynamics and Materials Conference, Honolulu, HW, United States, April 23–26, 2007. Volume 2, Pages 1503-1512, Year 2007.

Paper 2. GÄRDSBACK, M. AND TIBERT, G., 2008 Deployment control of spinning space webs. Accepted for publication in Journal of Guidance, Control and Dynamics. DOI: 10.2514/1.37468

Paper 3. GÄRDSBACK, M. AND TIBERT, G., 2008

Optimal deployment control of spinning space webs and membranes. Submitted to Journal of Guidance, Control and Dynamics.

Paper 4. GÄRDSBACK, M. AND TIBERT, G., 2007

A comparison of rotation-free triangular shell elements for unstructured meshes.

Computer Methods in Applied Mechanics and Engineering, Volume 196, Issues 49-52, Pages 5001-5015, Year 2007. DOI: 10.1016/j.cma.2007.06.017

Division of work between authors

Paper 1. This paper is a short version of a more extensive external report, but with focus on the simulation part. The project, that the paper and report are based on, was initiated by Leopold Summerer and Dario Izzo at the ESA Advanced Concepts Team. Gunnar Tibert (GT) conducted the work at KTH Mechanics, wrote most of the report, performed the design and folding analysis, developed the MATLAB code for the folding of the space web and proposed to use the analytical model. Mattias Gärdsback (MG) implemented and further developed the analytical model, developed the rest of the MATLAB and LS-DYNA code, performed the simulations and analysis, and wrote this paper and the simulation part of the report. The two authors discussed and planned the content of the paper together and MG wrote it.

Paper 2. This article is further developed from **Paper 1**. The distribution of work was different because more focus was on the simulations. GT initiated the work and wrote parts of the introduction and a larger part of the control system section. MG performed the simulations and analysis, and wrote most of the article.

Paper 3. MG initiated the work, performed the simulations and analysis, and wrote the article. GT contributed with important ideas and discussion.

Paper 4. The work on rotation-free elements was initiated by GT, who also contributed with many important ideas during the work. The coding and analysis was performed by MG, who also wrote the article.

The papers are re-set in the present thesis format